LA-14271-T
Thesis

The Sorption/Desorption Behavior of Uranium in Transport Studies Using Yucca Mountain Alluvium

Los Alamos
NATIONAL LABORATORY
EST. 1943

The World's Greatest Science Protecting America

This thesis was accepted by the Department of Chemical Engineering, The University of New Mexico, Albuquerque, New Mexico, in partial fulfillment of the requirements for the degree of Master of Science. The text and illustrations are the independent work of the author, and only the front matter has been edited by the IM-1 Writing and Editing Staff to conform with Department of Energy and Los Alamos National Laboratory publication policies.

Los Alamos National Laboratory, an affirmative action/ equal opportunity employer, is operated by the University of California for the United States Department of Energy under contract W-7405-ENG-36.

LA-14271-T
Thesis
Issued: February 2006

The Sorption/Desorption Behavior of Uranium in Transport Studies Using Yucca Mountain Alluvium

Cynthia D. Scism

Los Alamos
NATIONAL LABORATORY
EST. 1943

The World's Greatest Science Protecting America

SORPTION/DESORPTION BEHAVIOR OF URANIUM IN TRANSPORT STUDIES USING YUCCA MOUNTAIN ALLUVIUM

BY

CYNTHIA D. SCISM

B.S. ENVIRONMENTAL SCIENCE, UNIVERSITY OF HOUSTON-CLEAR LAKE, 2001

THESIS

Submitted in Partial Fulfillment of the
Requirements for the Degree of

Master of Science
Chemical Engineering

The University of New Mexico
Albuquerque, New Mexico

December, 2005

Cynthia D. Scism
Candidate

Chemical Engineering
Department

This thesis is approved, and it is acceptable in quality and form for publication on microfilm:

Approved by the Thesis Committee:

_____, Chairperson

_____

_____

_____

_____

_____

_____

Accepted:

_____
Dean, Graduate School

_____
Date

ACKNOWLEDGEMENTS

Financial support for this research was provided by the U.S. Department of Energy through the Office of Civilian Radioactive Waste Management Science and Technology Program at Los Alamos National Laboratory. Special thanks to my mentor and research advisor at Los Alamos National Laboratory, Dr. Paul Reimus, whose ideas resulted in an interesting research project and will ultimately make important contributions to the site characterization of Yucca Mountain. I would like to thank my research and academic advisor at the University of New Mexico, Dr. Eric Nuttall. His guidance, understanding and patience in helping me attain my research and academic goals were instrumental in the completion of my thesis and degree plan. I would also like to thank my committee members Dr. Laura Crossey and Dr. Steve Cabaniss for their valuable input in the fields of geochemistry and environmental chemistry.

I would like to thank my co-workers at Los Alamos National Laboratory, Dr. Mei Ding and Doug Ware, for sharing with me their invaluable technical experience in column and batch sorption studies and Steve J. Chipera for Quantitative X-ray Diffraction analyses. I would like to thank Mike Spilde of the Earth and Planetary Sciences at the University of New Mexico for providing his expert technical support for the Electron Probe Microanalysis that made my thesis even more interesting and colorful. Last, but not least, I would like to thank those who put up with me during my pursuit of this degree including my office mate and friend Kate Jones, who is always up for a good technical discussion, and last but not least, my family.

SORPTION/DESORPTION BEHAVIOR OF URANIUM IN TRANSPORT STUDIES USING YUCCA MOUNTAIN ALLUVIUM

BY

CYNTHIA D. SCISM

ABSTRACT OF THESIS

Submitted in Partial Fulfillment of the
Requirements for the Degree of

Master of Science
Chemical Engineering
The University of New Mexico
Albuquerque, New Mexico

December, 2005

The Sorption/Desorption Behavior of Uranium in Transport Studies Using Yucca Mountain Alluvium

by

Cynthia D. Scism

B.S., Environmental Science, University of Houston-Clear Lake, 2001

M.S., Chemical Engineering, University of New Mexico, 2005

ABSTRACT

Yucca Mountain, Nevada is the proposed site of a geologic repository for the disposal of spent nuclear fuel and high-level radioactive waste in the United States. In the event repository engineered barriers fail, the saturated alluvium located south of Yucca Mountain is expected to serve as a natural barrier to the migration of radionuclides to the accessible environment. The purpose of this study is to improve the characterization of uranium retardation in the saturated zone at Yucca Mountain to support refinement of an assessment model.

The distribution of uranium desorption rates from alluvium obtained from Nye County bore holes EWDP-19IM1, EWDP-10SA, EWDP-22SA were studied to address inconsistencies between results from batch sorption and column transport experiments. The alluvium and groundwater were characterized to better understand the underlying mechanisms of the observed behavior.

Desorption rate constants were obtained using an activity based mass balance equation and column desorption experiments were analyzed using a mathematical model utilizing multiple sorption sites with different first-order forward and reverse reaction rates. The uranium desorption rate constants decreased over time, suggesting that the alluvium has multiple types of active sorption sites with different affinities for uranium. While a significant fraction of the initially sorbed uranium desorbed from the alluvium quite rapidly, a roughly equivalent amount remained sorbed after several months of testing. The information obtained through this research suggests that uranium may experience greater effective retardation in the alluvium than simple batch sorption experiments would suggest.

Electron Probe Microanalysis shows that uranium is associated with both clay minerals and iron oxides after sorption to alluvial material. These results provide further evidence that the alluvium contains multiple sorption sites for uranium.

TABLE OF CONTENTS

LIST OF FIGURES

LIST OF TABLES

1. INTRODUCTION

1.1. Research Objectives

Yucca Mountain, Nevada is the proposed site for the development of a geologic repository for disposal of spent nuclear fuel and high-level radioactive waste. To obtain a license to construct and operate the proposed repository, the Yucca Mountain Project must demonstrate that the facility will meet radiation protection standards established by the U.S. Nuclear Regulatory Commission and the US Environmental Protection Agency (Eddebbarh et al. 2003). To isolate radioactive waste from the accessible environment, the repository will rely on a system of both engineered and natural barriers. Of concern to the overall performance assessment of the repository is the transport of radionuclides by groundwater through the subsurface to the accessible environment. The saturated alluvium south of Yucca Mountain is an important contributor to repository performance that will serve as a final barrier to retard the migration of radionuclides; delaying transport and reducing radionuclide concentrations at the compliance boundary. The accessible environment begins at the 18 km compliance boundary, which is the boundary beyond which compliance with radiation standards must be demonstrated.

To estimate the contribution of the saturated alluvium at Yucca Mountain to the overall performance of the repository; batch, column and in situ field transport studies are performed on the alluvium to determine its ability to retard the migration of radionuclides. Previous laboratory transport studies have shown inconsistencies between uranium batch sorption and column transport experimental results. Specifically, batch sorption experiments suggest a much later breakthrough time than

the early breakthrough of a portion of the radionuclide mass observed in some column transport experiments. This early breakthrough is not consistent with slow first-order sorption kinetics, so another explanation for the inconsistent transport behavior must be sought.

We hypothesize that uranium transport can be more effectively modeled by using a continuous or discretized distribution of desorption rates. Experiments have been designed to both measure (batch experiments) and validate (column experiments) such distributions. In general, the experiments performed as a part of this research will support the development of better models for contaminant transport in heterogeneous porous media.

The specific tasks completed as a part of this research were:

- Determination of the major and trace mineralogy of the alluvium using Quantitative X-ray Diffraction and iron oxide extraction methods to develop possible correlations between uranium sorption and major and minor mineral phases present in the alluvium;
- Evaluation of the retardation potential of alluvium for uranium in batch sorption and multi-step batch desorption experiments using alluvium samples and water collected from boreholes in saturated alluvium along potential flow pathways to the accessible environment;

- Determination of the distribution of desorption rates of uranium by a continuous flow desorption technique using the same water and alluvium as in the batch sorption experiments;
- Derivation of a mass balance equation for the desorption columns to obtain desorption rates throughout the desorption process;
- Demonstration of the applicability of a multi-site, multi-rate model for the transport of uranium in Yucca Mountain alluvium by fitting the column desorption data with an appropriate mathematical model;
- Investigation of the possibility of multiple sorption sites for uranium using electron probe microanalysis to determine uranium elemental associations in alluvial thin sections with sorbed uranium.

1.2. Background

1.2.1. Previous Uranium Transport Studies

The uranium transport studies described below were performed by the author and colleagues in support of the Yucca Mountain Project. The observations made during these studies give the necessary background and premise for the present study. A review of the literature is also made to provide additional background and support the present study.

Sorption Studies. Uranium batch sorption experiments using alluvium and groundwater from the three wells used in the present study indicate that the distribution coefficient, K_d (ml/g) of uranium at equilibrium with the alluvium varies from 1.7 to 23 ml/g (Figure 1.1). The batch experiments were conducted on three separate sieved particle size fractions of the alluvium (500-2000, 75-500 and <75 micrometers) under ambient pressure and temperature conditions. In each case, the smallest size fraction exhibited the greatest affinity for the uranium tracer solution.

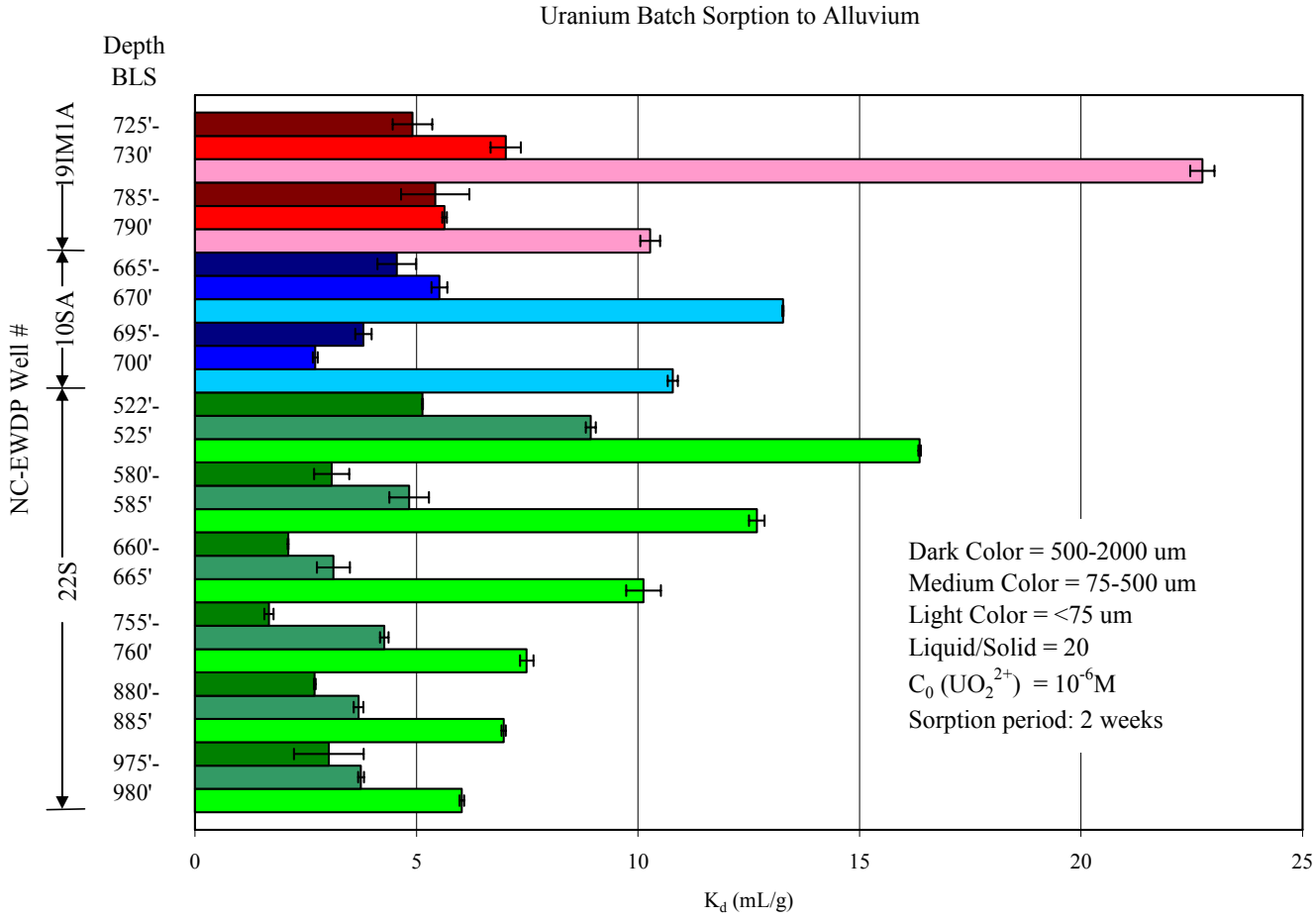

Figure 1.1. Batch Sorption Of Uranium To Alluvium As A Function Of Particle Size And Depth. The smaller size fractions tend to have the greatest affinity for uranium. The partitioning coefficient, K_d ranges from 1.7 to 23 mL/g.

Laboratory Dynamic Transport Studies. As a complement to the batch sorption experiments, uranium transport experiments were carried out under fully-saturated conditions and continuous-flow in columns packed with alluvium used in the batch experiments (weight percentages of 75-500 μm and 500-2000 μm size fractions kept the same as in original alluvium composite material). The column experiments were conducted with uranium as a reactive tracer and tritiated water (^{3}HHO) as a conservative tracer under ambient conditions. The tracers were delivered simultaneously as a pulse injection once steady state flow conditions had been reached. The initial elution rate for the columns was 10 ml/hr, decreasing to 5 ml/hr and then very quickly to 3 ml/hr as the experiments progressed. Table 1.1 outlines the experimental materials and parameters for each column. The uranium breakthrough curves relative to tritium are shown in Figures 1.2-1.4. In all cases, a small fraction of the uranium broke through at almost the same time as the tritium, but the vast majority of the uranium mass was significantly retarded. Total uranium recoveries ranged from 26 to 65 percent of the injected uranium, although mass was still being recovered when the experiments were stopped. The long tails and incomplete recoveries observed in the column experiments indicate that some of the uranium was slow to desorb from the columns within the time frame of the experiments. A long-tailing curve may also indicate the presence of stagnant areas and preferential flow within the column (Schweich and Sardin 1981), but this possibility can be ruled out because the tritium did not exhibit this behavior. Also shown in Figures 1.2-1.4 are CXTFIT predicted breakthrough curves based on retardation factors calculated using Equation 1.1 below. The K_d values are calculated

from the batch sorption experiments conducted with alluvium from the same well and screened interval as in the column experiments. The K_d values are weighted based on weight percent of 75-500 μm and 500-2000 μm size fractions used in the column experiments. Column dispersion (D) and velocity (v) were estimated by CXTFIT using the tritium breakthrough data for each column.

Table 1.1. Uranium Column Experiments

	Column #1	Column #2	Column #3
Well alluvium collected from	19IM1A	10SA	22SA
Interval (ft. BLS)	725-730	665-670	522-525
Particle Size (μm)	75-2000	75-2000	75-2000
Well Water Used	19D-Zone 1	10SA	19D Zone 1
pH range	8.4-8.7	8.2-8.5	8.4-8.7
Dry alluvium packed in column (g)	374.61	356.59	390.72
Water weight after saturation (g)	89.82	102.4	85.98
Porosity	.41	.44	.39

Note: The length of columns 1, 2 and 3 are 45, 46 and 45 cm, respectively and the diameter for each is 2.5 cm. The initial flow rate for all three columns is 10 m/hr.

It is important to note that the CXTFIT curves were generated using weighted K_d values for the alluvium over the particle size range of 75 μm to 2000 μm because the columns did not contain materials less than 75 μm in size. Particles less than 75 μm would wash out of the column ends and potentially clog the column bed supports and therefore are wet sieved from the 75 μm to 2000 μm alluvium fractions before packing the columns. Although the <75 μm size fraction has the smallest weight percent of each alluvium (≈2-2.5 wt.%), the uranium batch sorption K_d values for this fraction tends to be higher and may potentially have a large effect on transport.

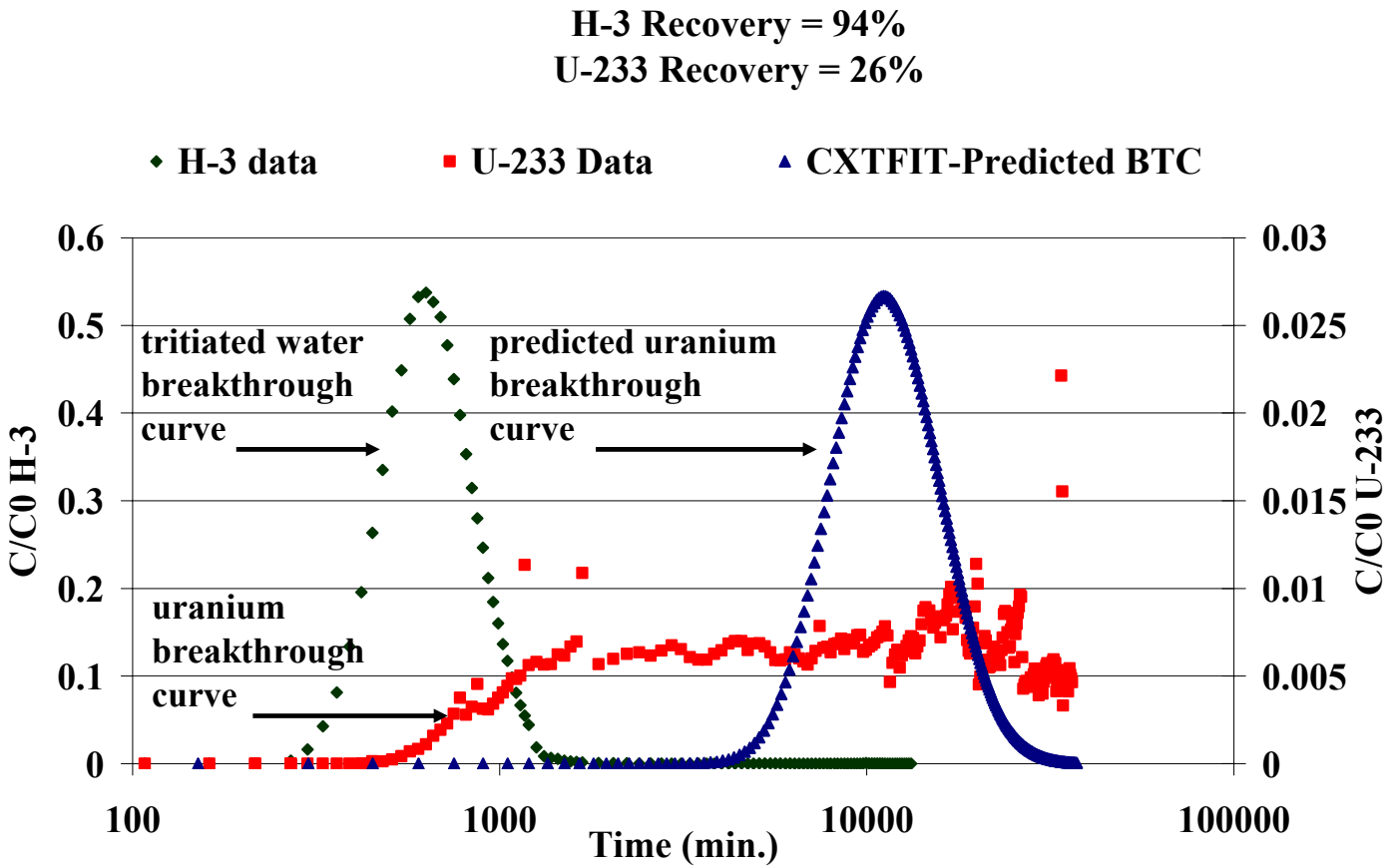

Figure 1.2. Breakthrough Curves For 19IM1A Alluvium Column Experiment And CXTFIT Predicted BTC For Uranium Based On Kd From Batch Studies. Note that tritium breakthrough is on the left axis and uranium breakthrough, including CXTFIT predicted uranium breakthrough is on the right axis.

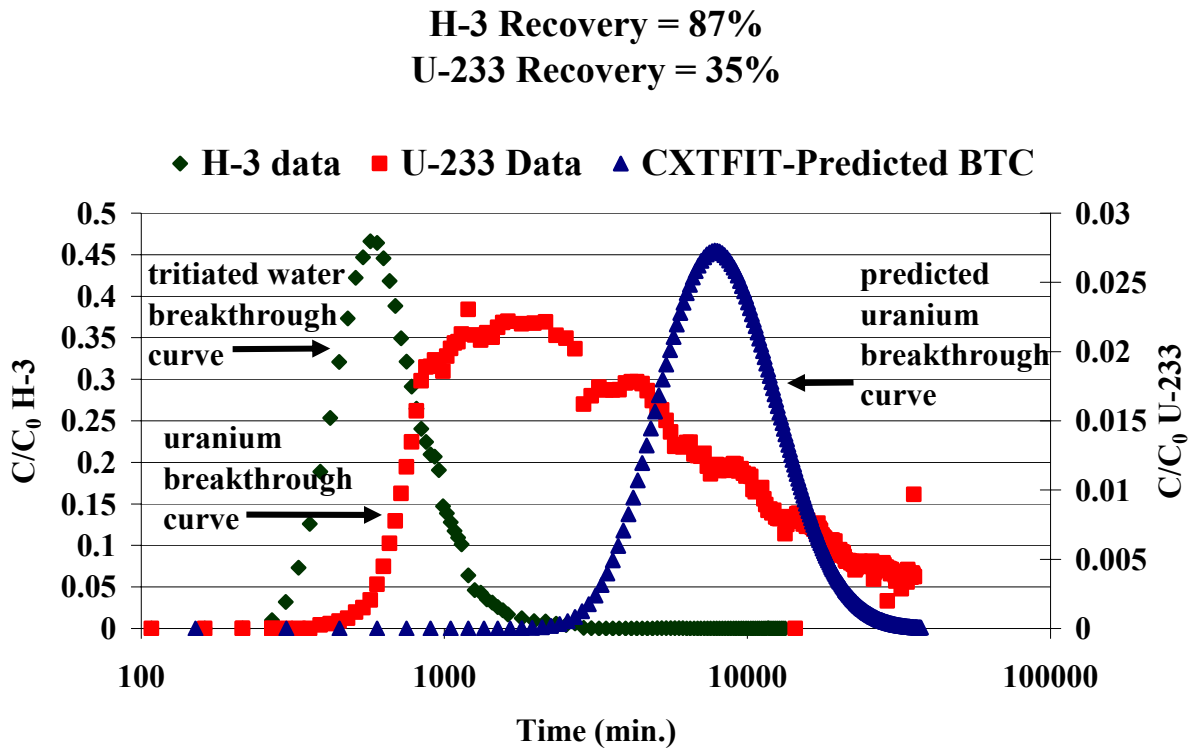

Figure 1.3. Breakthrough Curves For 10SA Alluvium Column Experiment And CXTFIT Predicted BTC For Uranium Based On Kd From Batch Studies. Note that tritium breakthrough is on the left axis and uranium breakthrough, including CXTFIT predicted uranium breakthrough is on the right axis.

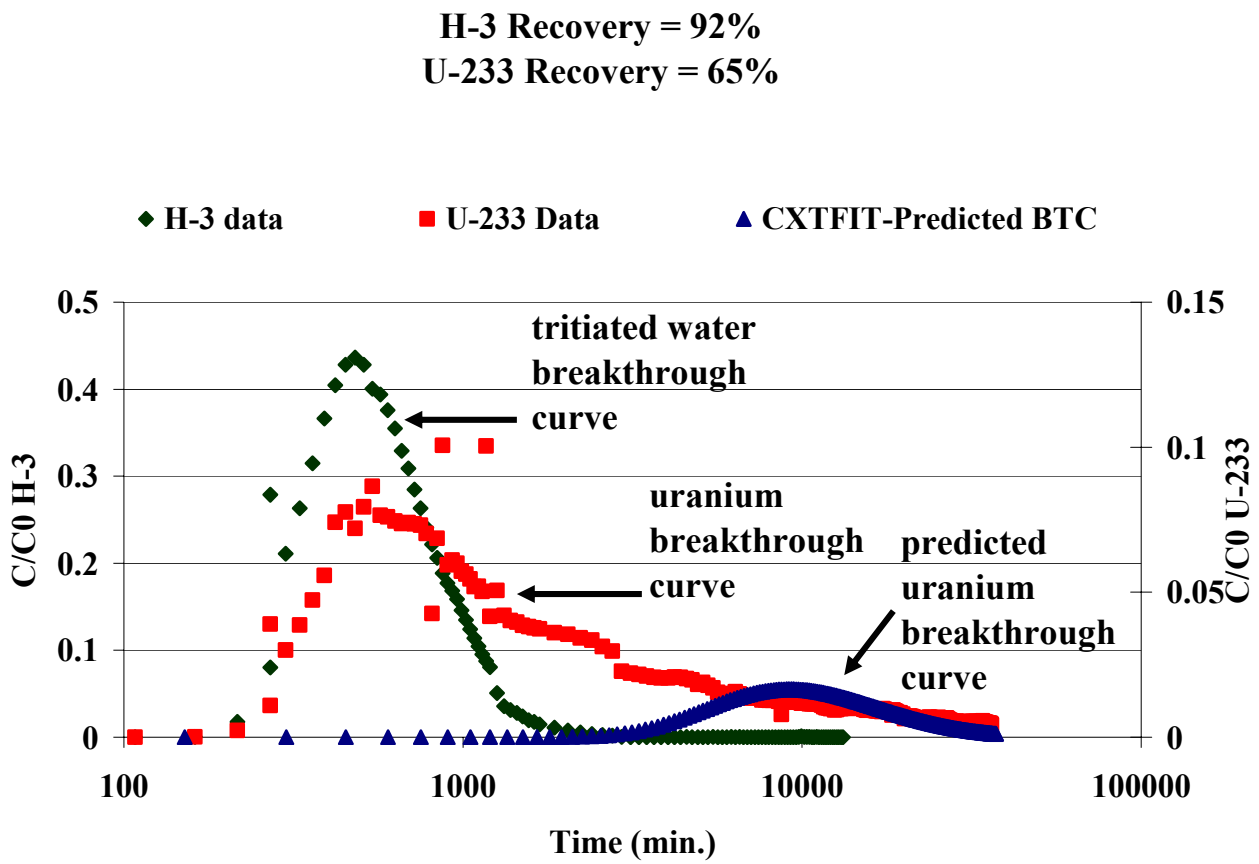

Figure 1.4. Breakthrough Curves For 22SA Alluvium Column Experiment And CXTFIT Predicted BTC For Uranium Based On Kd From Batch Studies. Note that tritium breakthrough is on the left axis and uranium breakthrough, including CXTFIT predicted uranium breakthrough is on the right axis.

If the sorption of uranium onto the saturated alluvium followed a linear sorption isotherm with fast sorption and desorption kinetics, the breakthrough curve would resemble that of a conservative tracer (in this case tritium), but would be delayed by a retention factor *R* (Stumm 1992) as shown by the CXTFIT curves in Figures 1.2-1.4:

$$R = 1 + \left(\frac{\rho}{\theta} \right) K_d \qquad \text{(Equation 1.1)}$$

R = retardation factor

ρ = dry bulk density of the alluvium in the column

θ = porosity of the column (under fully saturated conditions)

K_d = batch partition coefficient

The column experiments do not correlate well with the batch experiments in that the column transport of uranium could not be explained by either slow sorption kinetics or equilibrium sorption with a single K_d value (i.e., a single sorption and desorption rate). Rather, the column experiments suggested a distribution of K_d values that appear to be governed by a distribution of desorption rates that resulted in a long-tailed response and incomplete recovery of uranium from the columns.

1.2.2. Effects of Water Chemistry on Uranium Speciation and Sorption

According to Prikryl, et. al. (1994) the water chemistry parameters most important in uranium adsorption to geologic media are pH, carbonate concentration and uranium concentration. Echevarria et. al. (2001) found uranium sorption to increase with increasing pH (ph 5.5-8.8) and the presence of uranyl-carbonate complexes at higher pH suppress sorption more than sorption is increased by greater clay and organic carbon

content. In addition to adsorption reactions, radionuclides may precipitate forming immobile solid phases on rock surfaces. For uranium, the redox condition of the system determines the extent to which precipitation will occur. In pure water at one bar of pressure between pH = 0 to 5.5 and Eh = 0.2V to -.06V or at pH 5.6 and Eh 0.1V decreasing to -.06V at pH 12 (see Langmuir (1997), Figure 13.8), the more soluble U(VI) would be reduced to U(IV) lowering the solubility of uranium in the groundwater (Morris 2002). The studies described herein were performed under ambient conditions and the groundwater/tracer solutions used in the experiments are assumed to be in equilibrium with the ambient atmosphere (oxidizing conditions, 0.033% CO_2). Eh measurements taken in the lab of groundwater and tracer solutions before and after sorption range from 0.1V to 0.4V. The uranium species that exist at Eh above 0.1V and at the pH of the groundwater/tracer solutions used in the experiments (pH >8) are $UO_2(OH)_3^-$, $UO_2(CO_3)_2^{2-}$ and $UO_2(CO_3)_3^{4-}$ (Langmuir 1997). Oxidizing groundwater should result in smaller K_d values for uranium compared to reducing groundwater where precipitation reactions would contribute to uranium removal from solution. Precipitation of uranium would not necessarily result in an increase in K_d value although, U(IV) species may sorb more strongly than U(VI) species when both are under-saturated, especially at pH above 7 where (U(VI) complexes with carbonate species dominate in solution. Waite et al. (1994) using an equilibrium speciation computer code, HYDRAQL, studied the aqueous speciation of uranium at $P_{CO_2} = 10^{-3.5} atm$ and $P_{CO_2} = 10^{-2} atm$. In equilibrium with air ($P_{CO_2}= 10^{-3.5}$), the aqueous speciation of uranium at pH near neutral to alkaline is dominated by uranyl carbonate species where as at $P_{CO_2} = 10^{-2} atm$ these species begin to dominate at lower pH (Waite et al. 1994). The dominant carbonate species in solution

over the pH range of this study do not vary for $P_{CO_2}= 10^{-3.5}$ and $P_{CO_2}= 10^{-2.0}$ (Langmuir 1997).

Competing Cations

Hsi (1981) found that calcium or magnesium (10^{-3}M) did not significantly affect uranyl adsorption to amorphous ferric oxyhydroxide, goethite, and natural hematite suspensions. Barnett et. al. (2000) found that percentage of sorbed uranium species in a soil decreased as the ionic strength increased from .01 to .1 M ($NaNO_3$). A comparison of uranium sorption in groundwater from two different zones from NC-EWDP-19D onto alluvium from the same wells used in the present study is presented in Figure 1.5. In each case the uranium sorption in the 19D Zone 1 water was greater. Although the ionic strength is higher in the Zone 4 water, it is not significantly different from Zone 1 and the results presented in Figure 1.5 are most likely attributable to the higher carbonate concentration in the Zone 4 water. A summary of the groundwater chemistry for each of the three waters is shown in Table 4.1 in Section 4.1.

1.2.3. Mineralogical Effects on Uranium Sorption

Major Mineralogy

Clay minerals are expected to sorb uranium to a greater extent and more strongly than other mineral phases due to their high surface area and negative surface charge. Previous batch sorption experiments performed by the author and colleagues suggest a positive correlation between the increased presence of smectite in the alluvium and sorption of uranium. Stammose et al. (1992) performed batch sorption measurements of uranium to purified clay materials for potential use as an engineered barrier in radioactive waste disposal. Surface complexation at hydroxyl groups and cation exchange within the

smectite lattice (creating a charge deficit at the surface) and at exposed edge sites are two mechanisms considered in their study. A one and two site cation exchange model fit the log of the K_d value as a function of pH ($NaClO_4$ =1M) quite well up to a pH of around 7. The poor fit above this pH is most likely due to the presence of uranyl carbonate species. Subsequent batch desorption of uranium indicated that uranium sorption to clay minerals is highly reversible. Reimus et. al. (2005) also performed batch sorption of uranium onto purified clay minerals at varying pH. The results were similar to Stammose in that sorption increased from a pH ≈ 3 up to around pH ≈ 6.5 and decreased toward more alkaline pH. Although there is a positive correlation between clay mineral content and sorption of uranium, water chemistry plays and important role in uranium sorption to clay minerals.

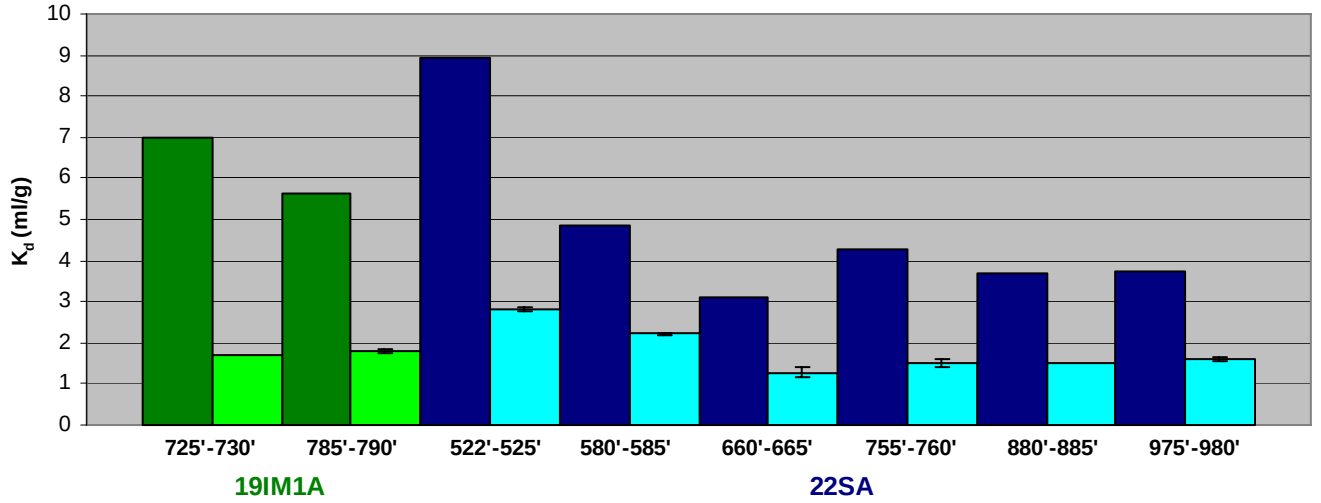

	pH	Alkalinity (as HCO_3) (mg/L)	Ionic Strength (I) (mol/L)
Darker Color: Well 19D Zone 1	8.60	189	4.378E-03
Lighter Color: Well 19D Zone 4	8.85	212	4.740E-03

Figure 1.5. Effect of Groundwater Chemistry on Sorption of Uranium by Alluvium. The dark green and blue color represents 19D Zone 1 data. The light green and blue represent 19D Zone 4 data. Experiments using the Zone 1 water consistently show greater sorption over Zone 4 water. Although ionic strength does not differ substantially between the two waters, other water chemistry parameters such alkalinity may be a contributing factor to the difference in sorption.

Trace Mineralogy

Iron or manganese oxide or hydroxide present in the alluvium as crystalline mineral phases or as amorphous coatings on mineral grains is expected to have a high affinity for heavy metals (Drever 1997). It has been shown by Hsi and Langmuir (1985) that Fe(III) oxyhydroxides play an important role in U(VI) adsorption. Their study also indicated that carbonate played a critical role in the distribution of U(VI) between the surfaces of iron oxide phases and solution. Gabriel, et. al. (1998) studied reactive transport of uranium in a goethite column. Their results indicated a non-linear adsorption isotherm that led them to believe that the reactions were kinetically controlled adsorption/desorption reactions. Microscopy performed by Stewart et. al. (2000) on pre and post leach roll-front uranium deposits indicate that uranium is widely associated with pyrite and pyrite partially dissolved by a mine leaching solution. Pyrite is known to reduce U(VI) to U(IV), thus decreasing solubility and increasing sorption.

Surface Area

Prikryl et. al. (1994) found that the total uranium sorbed increases as the sorbent-surface area/solution-volume ratio increases. Previous uranium batch sorption studies on alluvium from the same wells as the previous study separated into three particle size fractions (Figure 1.1) indicate that K_d increases from <75 μm > 75-500 μm > 500-2000 μm. Smaller particles sizes have greater surface area per unit mass resulting in increased properties such as surface charge or sorption site density per unit mass (Langmuir 1997). The increase in the surface charge and site densities results in an increase in uranium sorption per unit weight of material.

1.2.4. Influence of Natural Organic Matter and Microbial Processes on Uranium Sorption

Lenhart et. al. (1999) found that Uranium (VI) sorption to hematite in the presence of humic acid is increased at lower pH and decreases at more alkaline pH when compared to experimental sorption results of a binary Uranium (VI)/hematite system. Microbial activity may affect the solubility of uranium directly by enzymatic oxidation/reduction or biosorption. Microbes may also indirectly affect uranium sorption by changing the geochemistry of the system including pH and the formation of organic acids and chelates (Francis 1998). These processes can either precipitate uranium minerals, increasing retardation or cause mobilization of uranium, increasing transport. The survival and effectiveness of microbes is dependent on several factors (i.e. pH, redox conditions, and nutrients) and it is difficult to explain the effect that microbes may have on one system by studying another. Microbes and organics are not expected to play a significant role at Yucca Mountain because of the arid environment and deep water table.

1.2.5. Models of Uranium Sorption and Transport

Freundlich and Langmuir equations, cation exchange models and surface complexation models have been used successfully by Hsi and Langmuir (1985), Davis and Kent (1990) and many others to explain uranium sorption behavior in heterogeneous systems. Waite (1994) modeled the sorption of uranium by ferrihydrite using a surface complexation model with the equatorial oxygen atoms of uranium shared with the iron octahedron. Cation exchange models have often been used in an attempt to model uranium adsorption to heterogeneous materials, but in most cases these models do not capture the complex behavior of uranium sorption in these systems, especially at higher

pH (>7) (Stammose et al. 1992). Various transports codes such as FEHM (Finite Element Heat and Mass Transfer) have been used to do particle tracking of uranium species in the saturated zone at Yucca Mountain. These models consider only a singe K_d value for the partitioning of uranium between the solid and solution phases. This is a conservative approach to modeling uranium transport because K_d values assume reversible sorption, which tends to significantly underestimate radionuclide sorption parameters. Desorption rates likely control radionuclide fate and transport to a much greater degree than sorption rates.

Based on the available background information, it is expected that uranium sorption to Yucca Mountain alluvium will be dominated by surface complexation of uranyl ions that are present in solution predominantly as uranyl carbonate complexes. The sorption/desorption equilibrium and rates are expected to depend most strongly on groundwater pH and alkalinity as well as on clay and iron oxide content of the alluvium.

1.3. Scope of Work

The primary objective of the current study is to investigate the distribution of desorption rate constants of uranium from Yucca Mountain alluvium. In addition, the alluvium and groundwater are characterized to study correlations of uranium sorption and desorption behavior with parameters such as mineralogy, iron oxide content and water chemistry. This study does not include the effects of Natural Organic Mater (NOM) or microbes on sorption/desorption behavior of uranium because concentrations of these constituents are insignificant at Yucca Mountain due to the deep water table and the arid environment that supports little plant growth.

2. MATERIALS AND METHODS

2.1. General Approach

The primary objective was investigation of the distribution of desorption rate constants of uranium from Yucca Mountain alluvium. This was accomplished by performing uranium sorption experiments followed by a multi-step batch desorption technique and a continuous flow desorption technique. In addition, the effects of water chemistry on sorption and desorption was studied using two groundwater samples of varying water chemistry in paired experiments. The alluvium was characterized to quantify minerals such as clays, zeolites, iron oxide, silica, and alumina to investigate possible correlations with sorption/desorption behavior. Finally, alluvium thin sections with sorbed uranium were analyzed using electron probe microanalysis to investigate uranium sorption to mineral phases as well as amorphous coatings on minerals.

2.2. Materials

Alluvium

Alluvium samples were selected based on previous batch experiments that reflected higher partition coefficients (K_d values) at shallower depth intervals in the <75μm alluvium particle size range (Figure 1.1). A description of the alluvium samples is provided in Table 2.1. Secondary selection criteria was based on amount of alluvium material available for both batch and column experiments. A map of the test area showing the location of the Nye County wells is attached as Appendix 1. To provide support for well site selection Appendix 1 also contains a map showing predicted flow paths from the proposed repository site. Appendix 2-A, 2-B and 2-C are Summary

Lithology Logs for 19IM2A (in close proximity to 19IM1A), 22SA and 10SA respectively.

Table 2.1. Alluvium Depth Intervals and Sample Preparation Methods

Well Identifier	Depth (ft BLS)*	Sample Preparation Method	Particle Size Fraction (wt %)
NC-EWDP-19IM1A	740.0-745.0	dry sieve	75-2000 _m (re-combined)
NC-EWDP-22SA	557.0-560.0	dry sieve	75-2000 _m (recombined)
NC-EWDP-10SA	680.0-685.0	dry sieve	75-2000 _m (re-combined)

*Depth in feet below land surface

Groundwater

Water used for preparation of tracer solutions for batch and column experiments was taken from sample at well locations located in close proximity to or from wells which the alluvium samples in Table 2.1 were taken, with the exception of well location NC-EWDP-22SA. Groundwater from this well was unavailable and groundwater from Well 19D located adjacent to Well 19IM1A was used for the 22SA experiments. Groundwater from two different zones of NC-EWDP-19D with varying water chemistries was used with each of the 19IM1A and 22SA alluvium samples in the paired experiments. Water chemistry data are published on the Nye County Nuclear Waste Repository website (Nye County 2005) and the major ion chemistry for each water is provided in Table 4.1.

Radiotracers

A uranium tracer solution was prepared from a $UO_2(NO_3)_2$ stock solution diluted into the groundwaters described above. A concentration of $1x10^{-6}$ M was used as an extreme upper bound for a potential plume of uranium contamination.

2.3. Analytical Methods

2.3.1. Characterization of Alluvium

Surface area

Surface area of the dry alluvium samples were measured using the Brunauer Emmett Teller (BET) N_2 adsorption method with a NOVA 1200 high-speed gas sorption analyzer. The method uses a multi-point adaptation of the BET method (Brunauer 1938).

Iron content

Free iron oxides in the alluvium sample were extracted using the Citrate-dithionite Extractable Iron method of Loeppert and Inskeep (1996). The concentration of iron in the resulting extract was measured using Inductively Coupled Plasma-Atomic Emission Spectrometry (ICP-AES) following Environmental Protection Agency (EPA) Method 6010B (EPA 1996).

Mineralogy

Quantitative X-ray Diffraction (QXRD) was used to identify major mineral phases present in the alluvium. Quantitative mineral abundances were obtained from x-ray powder diffraction data using the FULLPAT procedure published by Chipera and Bish (2002).

Electron Probe Microanalysis

Electron Probe Microanalysis (EPMA) of alluvial thin sections with sorbed uranium was used to study the elemental associations of uranium with those present in the alluvium. A complete procedure for the EPMA analysis is attached as Appendix 5.

2.3.2. Uranium Analysis

After preparation, the uranium tracer solution was mixed with scintillation cocktail in a solution to cocktail ratio of 10:10 and its activity was measured using Liquid Scintillation Counting. The activity of the supernatant from batch experiments and the eluate from the column experiments was measured in the same manner. The percent sorbed or desorbed was calculated relative to the activity measured in the original tracer solution.

2.4. Experimental Design

2.4.1. Adsorption

Adsorption method. The batch adsorption method was employed for the experiments intended for multi-step desorption and column desorption techniques. The uranium tracer solution was added in a 5-7.5:1 Liquid:Solid ratio (ml/g) to polycarbonate Oak Ridge centrifuge tubes containing 4-6 grams of alluvium material as shown in Figure 2.1 from each of the three wells listed in Table 2.1. All samples were placed on a reciprocating shaker for two weeks and then centrifuged at 60 rpm to separate solids from solution. Control samples containing radiotracer but no alluvium were shaken and centrifuged with the samples containing alluvium to assess uranium sorption to centrifuge tube walls. The supernatant was analyzed by Liquid Scintillation Counting (LSC).

2.4.2. Multi-step Batch Desorption

Multi-step desorption. The multi-step batch desorption was initiated after two weeks of batch sorption by adding tracer-free groundwater to the alluvium remaining in the centrifuge tube after decanting the supernatant. The sample was returned to the reciprocating shaker for a period of one week at which time the solution was centrifuged

and the activity in the supernatant was analyzed. This procedure was repeated until the activity of the supernatant was no longer measurable by LSC.

2.4.3. Continuous Flow Desorption

Continuous flow (column) desorption. The column desorption of uranium was initiated after two weeks of batch sorption by placing the uranium-bearing alluvium (about 4 grams) into a column as shown in Figure 2.2. The alluvium partially fills the column, leaving room for approximately 10 mL of desorption solution (tracer-free groundwater) and enough head space to ensure that the desorption solution contact with alluvium is maximized. To create a well-mixed system and reduce concentration gradients in solution the columns were rotated end over end by a shaker throughout the desorption. A continuous flow of tracer-free ground water was delivered to the columns via syringe pumps. The eluate was collected in 8-10 ml fractions and the activity of the eluate was analyzed via Liquid Scintillation Counting (LSC). A digital photograph of the columns is shown in Figure 2.3. This procedure was continued until the activity of the eluate was not accurately measurable by LSC.

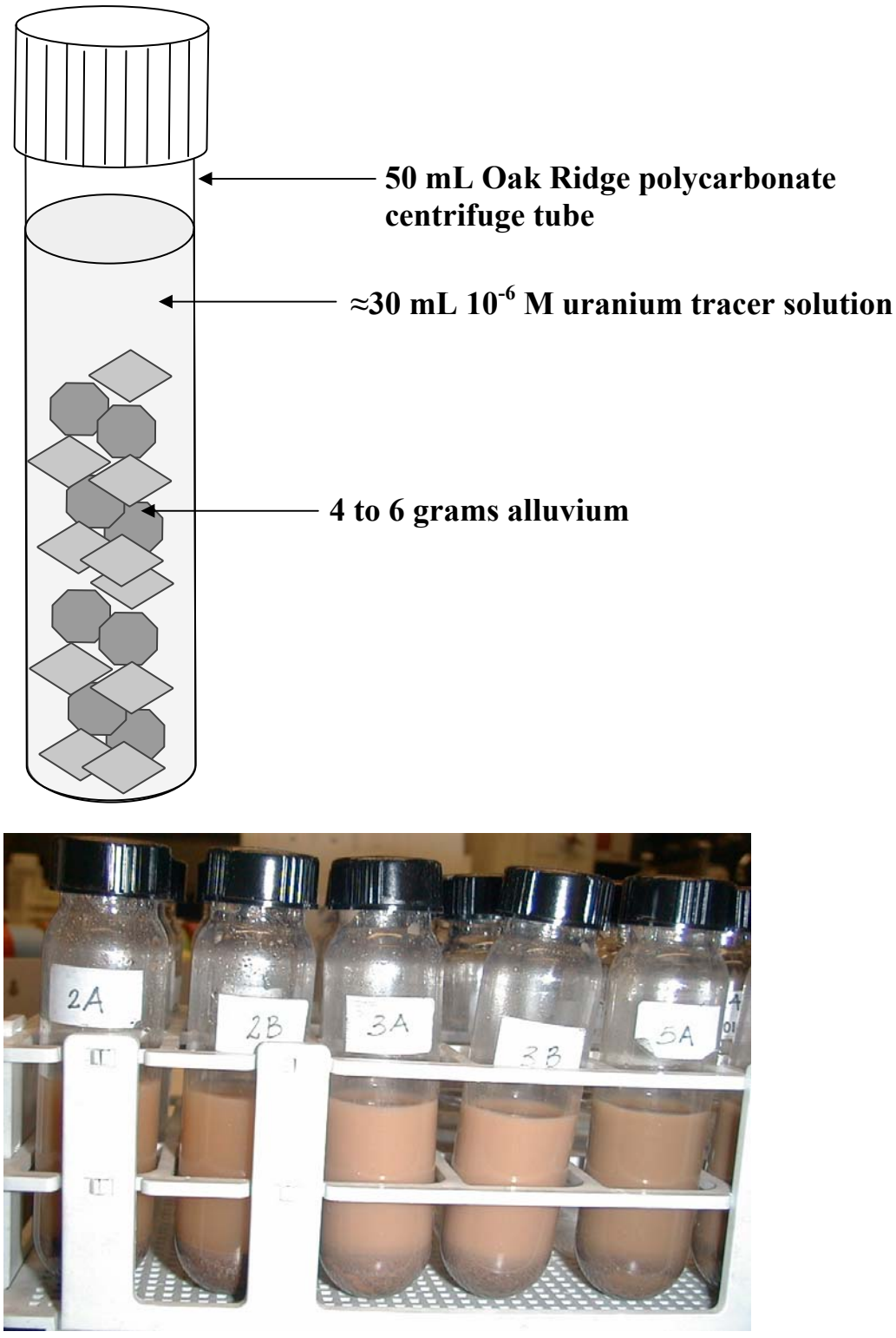

Figure 2.1. Schematic of Batch Sorption Tube and Digital Photograph of Batch Sorption Tubes.

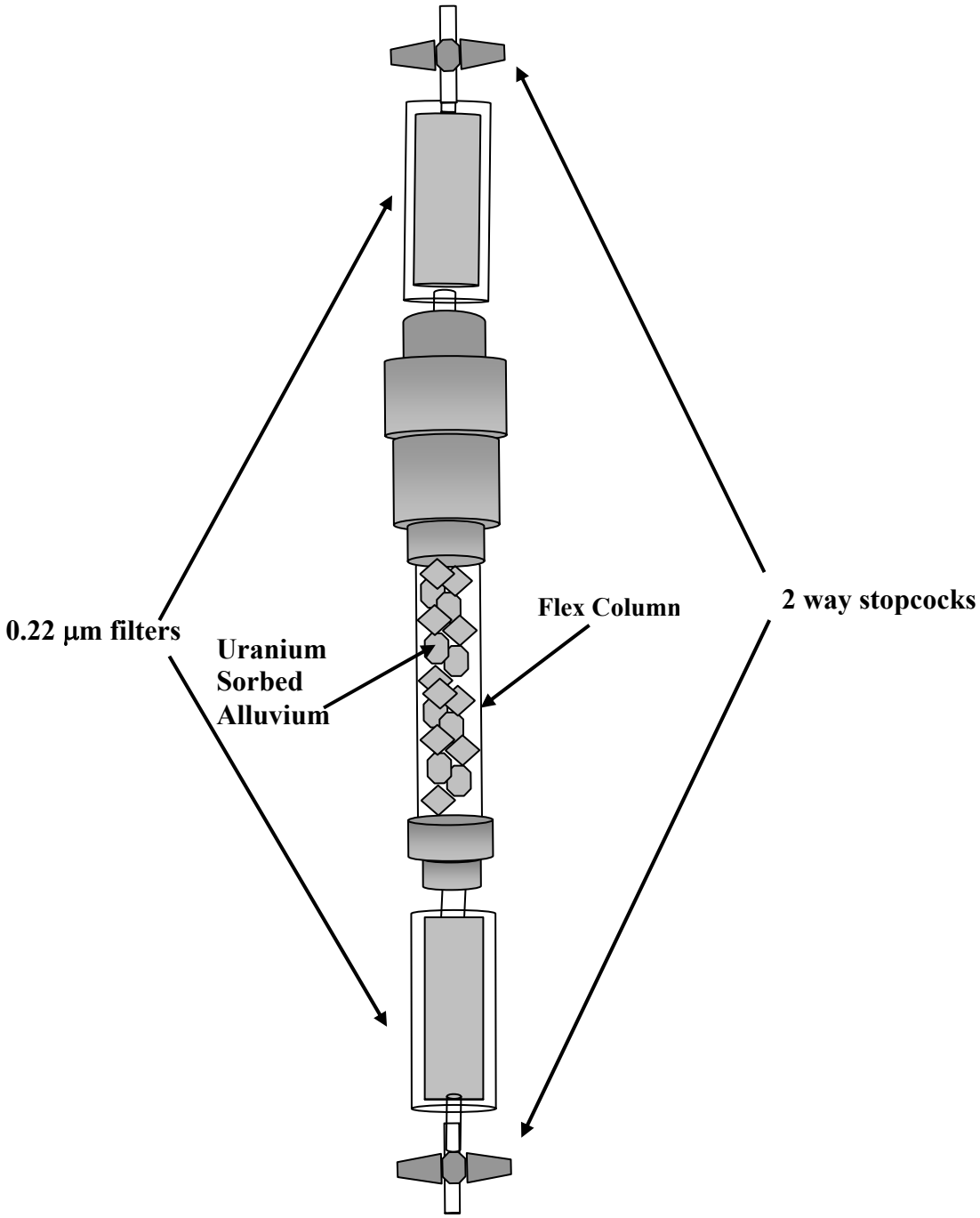

Figure 2.2. Schematic of Flow Desorption Column. The alluvium is pre-sorbed with uranium prior to the column flow desorption.

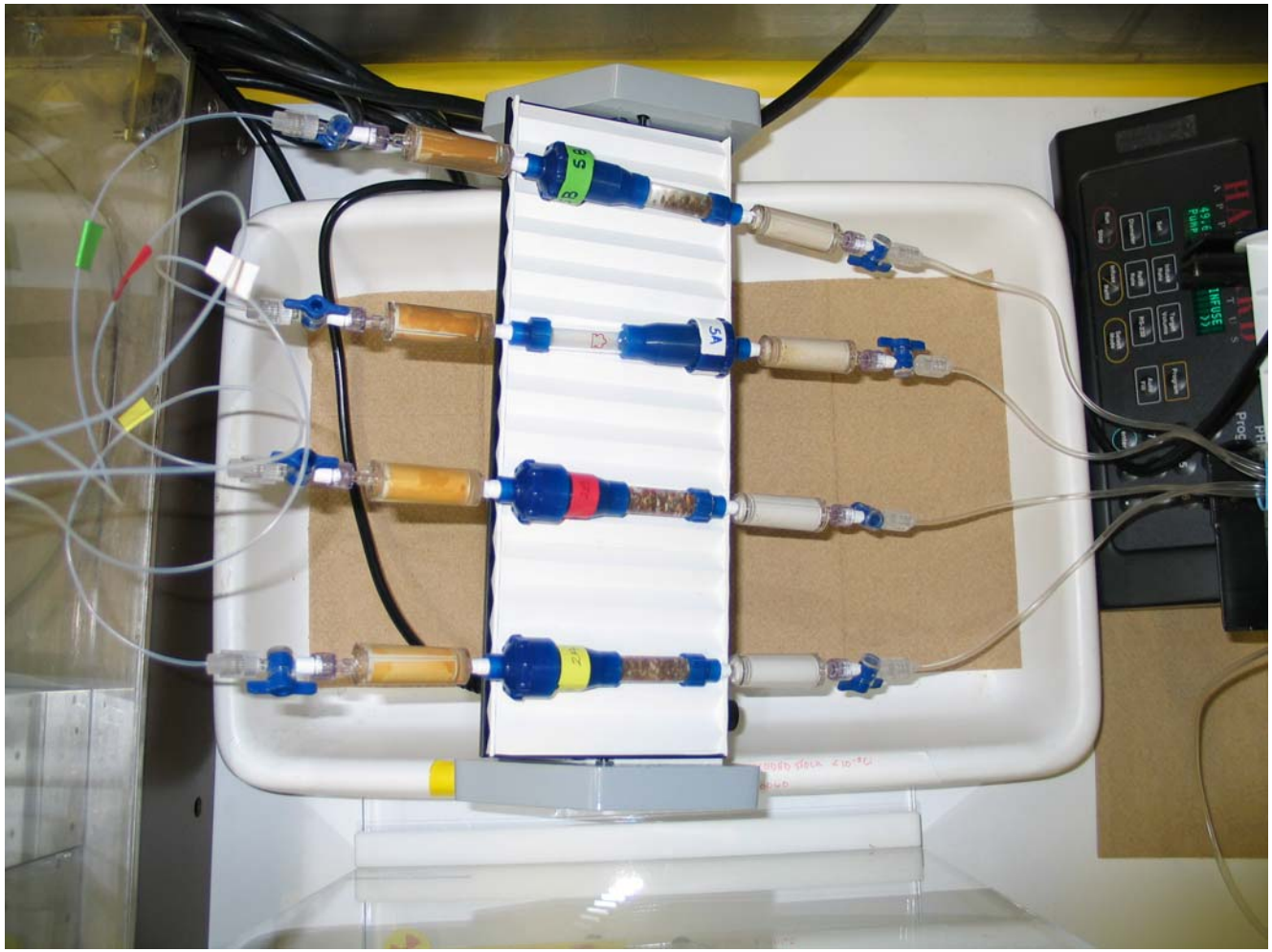

Figure 2.3. Digital Photograph of the Flow Desorption Columns.

3. INTERPRETIVE METHODS

3.1. Batch and Column Data Modeling

3.1.1. CXTFIT

The predicted uranium breakthrough curves in column transport experiments shown in Figures 1.2, 1.3, and 1.4 were modeled using the program CXTFIT. CXTFIT is a part of the STudio of ANalytical MODels [Simunek et al., 1999], a Windows-based computer software package for evaluating solute transport in porous media using analytical solutions of the convection-dispersion solute transport equation (Equation 3.1). The model parameters are based on retardation factors calculated using Equation 1.1 and K_d values from the batch sorption experiments conducted with alluvium from the same well and screened interval as in the column experiments. The K_d values are weighted based on weighted percents of 75-500 μm and 500-2000 μm size fractions used in the column experiments. Column velocity (v), bulk density (ρ) and porosity (θ) were calculated or measured for each column. Column dispersion (D) was estimated by fitting parameters to the tritium breakthrough data for each column using CXTFIT.

$$R\frac{\partial C}{\partial t} = D\frac{\partial^2 C}{\partial x^2} - v\frac{\partial C}{\partial x} \qquad \text{(Equation 3.1)}$$

R = Retardation Factor (Dimensionless)

C = concentration in the liquid phase (M/L^3)

D = solute dispersion coefficient (L^2/t)

v = mean pore-water velocity (L/t)

x = distance along the column (L)

t = time

3.1.2. Uranium Desorption Model

Column desorption experiments were analyzed using a mathematical model written in FORTRAN code utilizing multiple sorption sites with different first-order forward and reverse reaction rate constants. The adjustable parameters are sorption rate constant, desorption rate constant, number of different types of reaction sites, and maximum sorption capacity for each type of site. The model was used to fit the concentrations in samples collected from desorption columns as a function of time, allowing for flow rate changes and flow interruptions. Equations 3.2 and 3.3 below are used in the model to fit the experimental column desorption data.

(Equation 3.2)

$$\frac{dc}{dt} = \frac{1}{V}\left\{Q(C_{in} - C) - \left[k_1\left(1 - \frac{s_1}{s_{1\max}}\right) + k_2\left(1 - \frac{s_2}{s_{2\max}}\right) + k_3\left(1 - \frac{s_3}{s_{3\max}}\right) + k_4\left(1 - \frac{s_4}{s_{4\max}}\right) + k_5\left(1 - \frac{s_5}{s_{5\max}}\right)\right]C + k_{r1}s_1 + k_{r2}s_2 + k_{r3}s_3 + k_{r4}s_4 + k_{r5}s_5\right\}$$

(Equation 3.3)

$$\frac{ds_i}{dt} = \left[\frac{k_i\left(1 - s_i / s_{i\max}\right)C - k_{ri}s_i}{M}\right]$$

C = concentration out of column, CPM/mL

s_i = concentration sorbed to site i, CPM/g

C_{in} = concentration in solution flowing into column, CPM/mL

V = volume of solution in column, mL

Q = flow rate through column, mL/hr

M = mass of solid, g

k_i = forward rate constant for site i, mL/hr

k_{ri} = desorption rate constant for site i, g/hr

The experimental data was fit as closely as possible using one type of sorption site. Additional site types were added as necessary to improve the fit, while balancing the amount of uranium on the alluvium after the sorption step and the cumulative amount of uranium desorbed from the alluvium.

3.1.3. Calculation of reverse reaction rate constants k_r

The activity-based mass balance shown in Equation 3.4 was used to directly calculate instantaneous desorption rate constants for uranium from the alluvium.

$$\frac{dC}{dt} = \frac{k_r S}{V} - \frac{(q + k_f)C}{V} \quad \text{(Equation 3.4)}$$

S = CPM/g on solid

C = CPM/g in solution

q = flow rate (mL/hour)

V = volume of column (5-10 mL)

k_r = reverse rate constant (g/hr)

k_f = forward rate constant (mL/hr)

t= time in hours

Equation 3.4 can be rearranged to obtain the expression for k_r shown in Equation 3.5. k_fC is assumed to be negligible due to maximum sorption of uranium in the batch sorption step (q>>k_f).

$$k_r = \frac{V}{S}\left(\frac{dC}{dt}\right) + q\frac{C}{S} \quad \text{(Equation 3.5)}$$

4. RESULTS

4.1. Water Chemistry

The water chemistry data in Table 4.1 were used as input to PHREEQC-2 version 2.11 using the default database provided with the program. The ionic strength, bicarbonate concentration and calcite saturation index output for each groundwater is shown in Table 4.2. The ionic strength does not substantially vary between each groundwater and ranges from 3.029E-03 mol/L to 4.740E-03 mol/L increasing from 10SA<19D Zone 1<19D Zone 4. The bicarbonate concentration which is the dominant carbonate species ranges from 1.615E-03 mol/kg to 3.176E-03 mol/kg increasing from 10SA<19D Zone 1<19D Zone 4. Carbonate species concentrations are important in uranium sorption and desorption behavior due to the formation of uranyl carbonate complexes that increase the mobility of the uranyl ion. According to Langmuir (1997) at pH above 6 to 7 the uranyl carbonate species replace uranyl hydroxide species as the predominant solution species. Each of the three ground waters is under-saturated with respect to calcite. Calcite is not detected in the QXRD results in Table 4.4 for each of the three alluviums. If the groundwater were to come in contact with calcite, it would be reasonable to assume that it would dissolve in order to approach equilibrium. The output for the PHREEQC runs for each groundwater are attached as Appendix 3-A, 3-B and 3-C for 19D Zone 1, 19D Zone 4 and 10SA groundwater, respectively.

Table 4.1. Water Chemistry Data from Nye County Nuclear Repository Program Office, Early Warning Drilling Program Well Data.

	Well NC-EWDP-19D Zone 1	Well NC-EWDP-19D Zone 4	Well NC-EWDP-10SA
pH	8.6	8.85	7.78
Alkalinity (as HCO_3^-) (mg/L)	189	212	100
Ca^{2+} (mg/L)	3.7	0.92	13
Mg^{2+} (mg/L)	0.31	0.03	2.5
Na^+ (mg/L)	91.5	107.3	43
K^+ (mg/L)	3.7	3.4	5.2
Cl^- (mg/L)	6.1	5.6	6.9
SO_4^{2-} (mg/L)	22	18.7	14
NO_3^- (mg/L)	2.21	1.2	1.4

Table 4.2. Ionic Strength And Calcite Saturation Indices Calculated By PHREEQC For Water Chemistry Data From Nye County Nuclear Repository Program Office, Early Warning Drilling Program Well Data.

	Ionic Strength (I) (mol/L)	HCO_3^-/ CO_3^{2-} (m)	Saturation Index for Calcite (Log (IAP/K_{sp}))
Well NC-EWDP-19D Zone 1	4.378e-03	2.932e-03/6.743e-05	-0.02
Well NC-EWDP-19D Zone 4	4.740e-03	3.176e-03/1.309e-04	-0.36
Well NC-EWDP-10SA	3.029e-03	1.615e-03/5.444e-06	-0.49

4.2. Characterization of Alluvium

The surface area, iron oxides content and mineralogy of each re-combined (<75-2000 μm) alluvium sample is determined by the methods described in Section 2.3. The 22SA alluvium has a surface area almost three times that of both the 19IM1A and 10S alluviums and over twice the amount of iron oxides (Table 4.3). The iron oxides content of the alluvium appears to have some correlation with the smectite content of the samples (Table 4.4). Further testing would be required to confirm such a correlation. The QXRD results indicate that the clinoptilolite weight percent for 22SA and 10S alluvium is slightly higher than found in the 19IM1A alluvium and Smectite in the 22S sample is almost five times the weight percent found in the 19IM1A alluvium and over twice the weight percent found in 10SA alluvium. Due to the negative surface charge and high surface area of these mineral phases, smectite and clinoptilolite are expected to have a higher affinity for uranium than other mineral phases found in the alluvium.

Table 4.3. Alluvium Surface Area and Iron Oxide Content

	Surface Area (m^2/g)	FeOx (mg/g)	
		Concentration	Standard Deviation
NC-EWDP-191M1A	6.32	1.51	0.71
NC-EWDP-10SA	5.87	1.77	0.34
NC-EWDP-22SA	16.64	3.78	0.72

Table 4.4. Quantitative X-ray Diffraction-Mineralogy

Mineral Phase	Well NC-EWDP-191M1A (wt %)	Well NC-EWDP-22SA (wt %)	Well NC-EWDP-10SA (wt %)
Quartz	15.3	10.1	8.7
Plagioclase	23.0	28.4	26.0
K-Feldspar	24.4	17.5	30.6
Clinoptilolite $(Na, K, Ca)_{2-3}Al_3(Al, Si)_2Si_{13}O_{36}\text{-}12H_2O$	7.6	12.0	11.6
Mica	1.3	1.0	1.8
Kaolinite	0.5	0.2	0.4
Cristobalite	5.8	5.9	8.1
Tridymite	4.1	4.3	1.6
Opal-CT	13.6	---	---
Hematite	0.4	0.6	0.5
Smectite $(Na, Ca)(Al, Mg)_6(Si_4O_{10})_3(OH)_6 - nH_2O$	4.6	19.4	8.0
Total	100.6	99.4	97.4

4.3. Sorption Kinetics

To establish a batch sorption period adequate for uranium to reach equilibrium between the solid and solution phases in each of the five sample types, batch sorption experiments were carried out at one day, three days, one week, two weeks, three weeks and five weeks. The results in Figure 4.1 show that the amount of uranium adsorbed onto the alluvium changed little after one week, indicating that a batch sorption period of fourteen days is adequate for the batch and continuous flow desorption experiments.

Higher K_d values from the NC-EWDP-22SA alluvium may be the result of higher smectite and clinoptilolite content (Table 4.4). There also appears to be a correlation between iron oxide content in the NC-EWDP-22SA alluvium and sorption (Table 4.3).

4.4. Multi-step Desorption

To complement the continuous flow column desorption experiments, step-wise desorption experiments were carried out for each of the five samples after a sorption period of two weeks. The desorption was carried out over a period of 7 weeks, replacing the fresh groundwater in the centrifuge tube at one-week intervals and measuring the amount of activity in the removed solution by LSC. Multi-step desorption results (Figure 4.2) for U-233 from the three alluvium samples, including two-groundwater chemistries for 22S and 19IM1A alluvium samples, indicate similar desorption patterns although uranium desorbed from the alluvium ranges from sixty-four percent to seventy-six percent of the amount sorbed to the alluvium after the sorption phase.

The results show a higher rate of desorption in the initial four weeks when compared to the final four weeks. Over the five sample-water combinations five to twenty percent of the uranium originally in contact with the alluvium remained sorbed to the alluvium after eight desorption steps. The experimental results shown in Figures 4.1 and 4.2 are from separate sets of experiments, so the final and initial percent sorbed during the sorption (Figure 4.1) and desorption (Figure 4.2) phases, respectively, do not necessarily match.

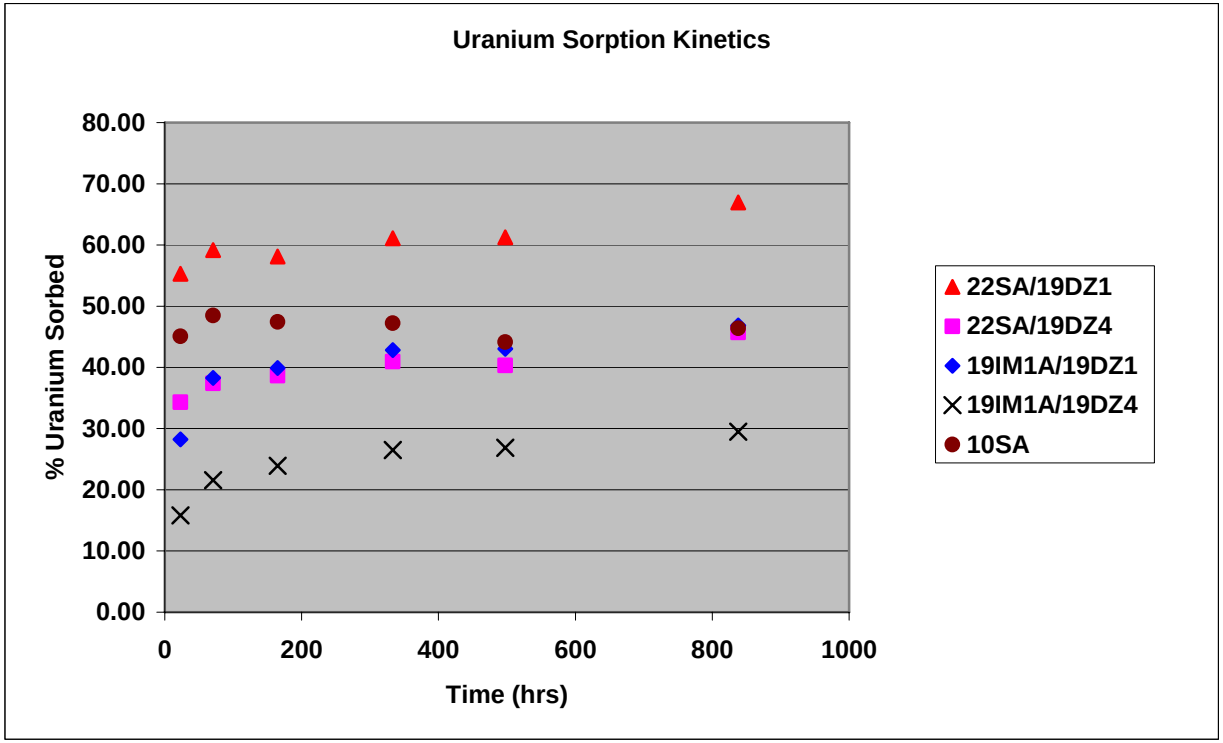

Figure 4.1. Uranium Sorption Kinetics. **Batch sorption experiments for each of five sample types was carried out at one day, three days, one week, two weeks, three weeks and five weeks to determine uranium partitioning equilibrium between the solid and solution phases at each time step. Note that experimental results shown in Figures 4.1 and 4.2 are from separate sets of experiments, so the final and initial percent sorbed during the sorption (Figure 4.1) and desorption (Figure 4.2) phases, respectively, do not necessarily match.**

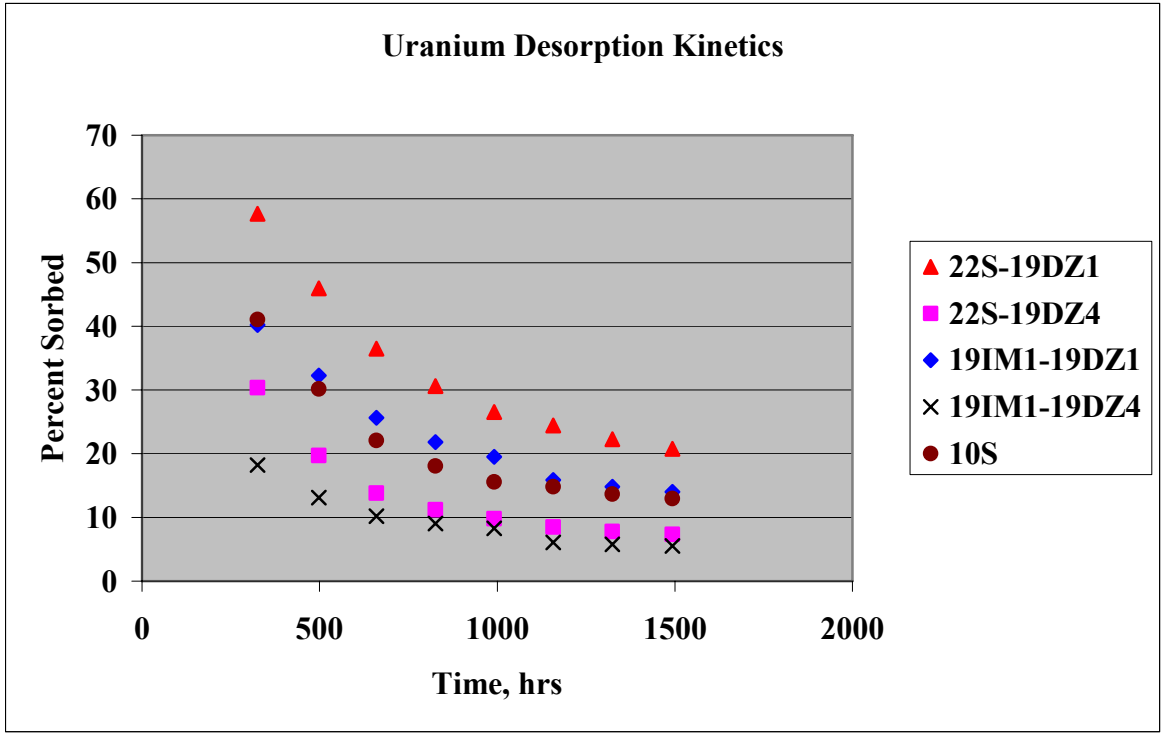

Figure 4.2. Uranium Desorption Kinetics. **Batch step desorption after a two-week sorption period for each of five sample types was carried out at one week intervals for a period of eight weeks to determine uranium partitioning equilibrium between the solid and solution phases at each desorption time step. Note that experimental results shown in Figures 4.1 and 4.2 are from separate sets of experiments so, the final and initial percent sorbed during the sorption (Figure 4.1) and desorption (Figure 4.2) phases, respectively, do not necessarily match.**

4.5. Continuous Flow Desorption

Uranium was desorbed from alluvium immediately after a batch sorption experiment was completed using a continuous flow of tracer-free groundwater through a small column (see method Section 2.4.3). Appendix 4 contains a detailed summary of the column desorption experiments presented in this section. The results in Table 4.5 and Figure 4.3, (a), (b) and (c) show the initial partitioning of uranium after a two-week batch sorption period (approximately 336 hours) and the subsequent partitioning during the desorption period. Figure 4.3(a) and 4.3(b) are results of duplicate runs (A & B) for alluvium from NC-EWDP-19IM1A (19IM1A) and NC-EWDP-22SA (22SA) and using both 19D Zone 1 and 19D Zone 4 groundwater. The duplicate runs are similar for the 19IM1A Zone 1, 22SA Zone 1 and 4 experiments. The 19IM1A Zone 4 and the 10SA (Figure 4.3(c)) duplicates show some variation in partitioning of the uranium throughout desorption. The column runs using the 19D Zone 1 water consistently result in a higher percentage of initial uranium sorption and greater partitioning of uranium to the solid phase during desorption than the experiments utilizing the 19D Zone 4 water. Although alluvium from 22SA has a higher initial partitioning of uranium on the solid phase than the 19IM1A alluvium in the 19D Zone 4 experiments, the partitioning of uranium on the solid phase of 19IM1A alluvium during desorption is either equal to or greater than that for the 22SA alluvium. In contrast, the 19IM1A alluvium has a lower initial partitioning of uranium on the solid phase than 22SA in the 19D Zone 1 experiments and the partitioning of uranium on the solid phase of 19IM1A alluvium during desorption is less than that for the 22SA alluvium. However, comparisons involving the 22SA-19D Zone 1 and 10SA results are

inconclusive due to early termination of these desorption experiments as a result of the Los Alamos National Lab stand-down beginning in June 2004.

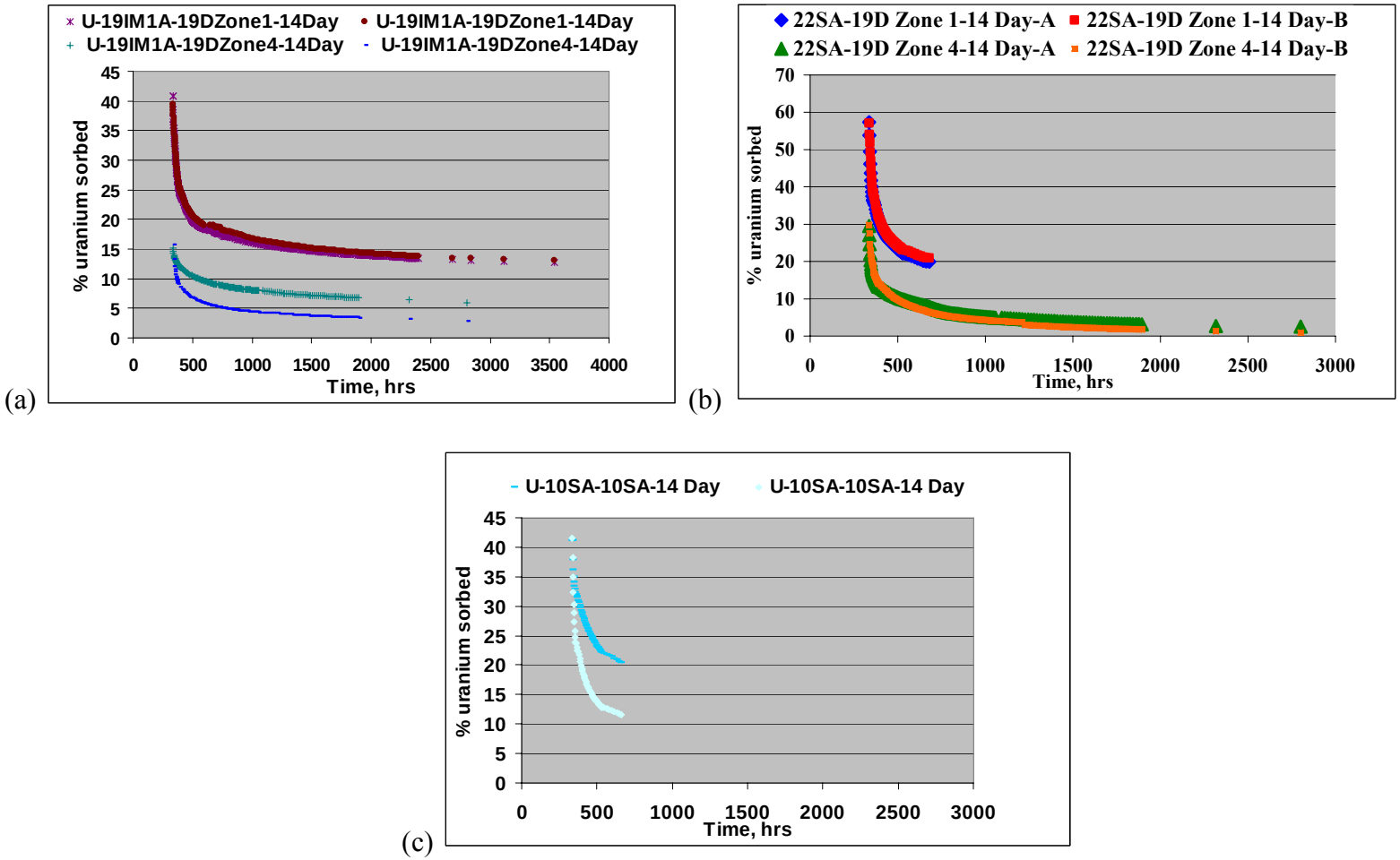

Figure 4.3. Partitioning of uranium as a function of time in alluvium desorption columns. Alluvium pre-sorbed with uranium is exposed to a continuous flow of fresh groundwater. The plots show percent of uranium that was originally placed in contact with alluvium remaining on alluvium over time (the first data point represents the percentage that was sorbed to the alluvium at the time desorption was started).

Table 4.5. Summary of Uranium Column Desorption Results.

Alluvium/Groundwater	Initial Amount of uranium sorbed	Amount of Sorbed uranium desorbed	Amount of initially sorbed uranium remaining on solid	Desorption Period (hours)
19IM1A /19D Zone 1-A	41%	69%	31%	3200
19IM1A /19D Zone 1-B	39%	67%	33%	3200
19IM1A/19D Zone 4-A	15%	60%	40%	2470
19IM1A/19D Zone 4-B	16%	83%	17%	2470
22SA/19D Zone 1-A	57%	65%	35%	336
22SA/19D Zone 1-B	57%	63%	37%	336
22SA /19D Zone 4-A	30%	91%	9%	2470
22SA /19D Zone 4-B	30%	95%	5%	2470
10S/10S-A	41%	50%	50%	336
10S/10S-B	41%	72%	28%	336

4.5.1. Uranium Desorption Model

The data obtained from column desorption experiments (CPM/g uranium desorbed over time) were analyzed using a mathematical model written in FORTRAN code utilizing multiple linear first-order forward and reverse reactions (sites) as described in Section 3.1.2. The column results and fits of the CPM/g uranium desorbed from the alluvium are shown in Figures 4.4-4.8 for each of the alluvium/groundwater combinations. A Summary of the modeling results are provided in Table 4.6.

Table 4.6. Summary of Input for Uranium Desorption Modeling.

Alluvium/Groundwater	Number of Sites	Range of Desorption Rate Constants (g/hr)	Desorption Period (hours)
19IM1A /19D Zone 1	4	.07 - .000001	3000
19IM1A/19D Zone 4	3	.04 - .0001	2136
22SA/19D Zone 1	2	.18 - .02	700
22SA /19D Zone 4	4	.4 - .0001	2136
10S/10S	2	.04 - .0025	700

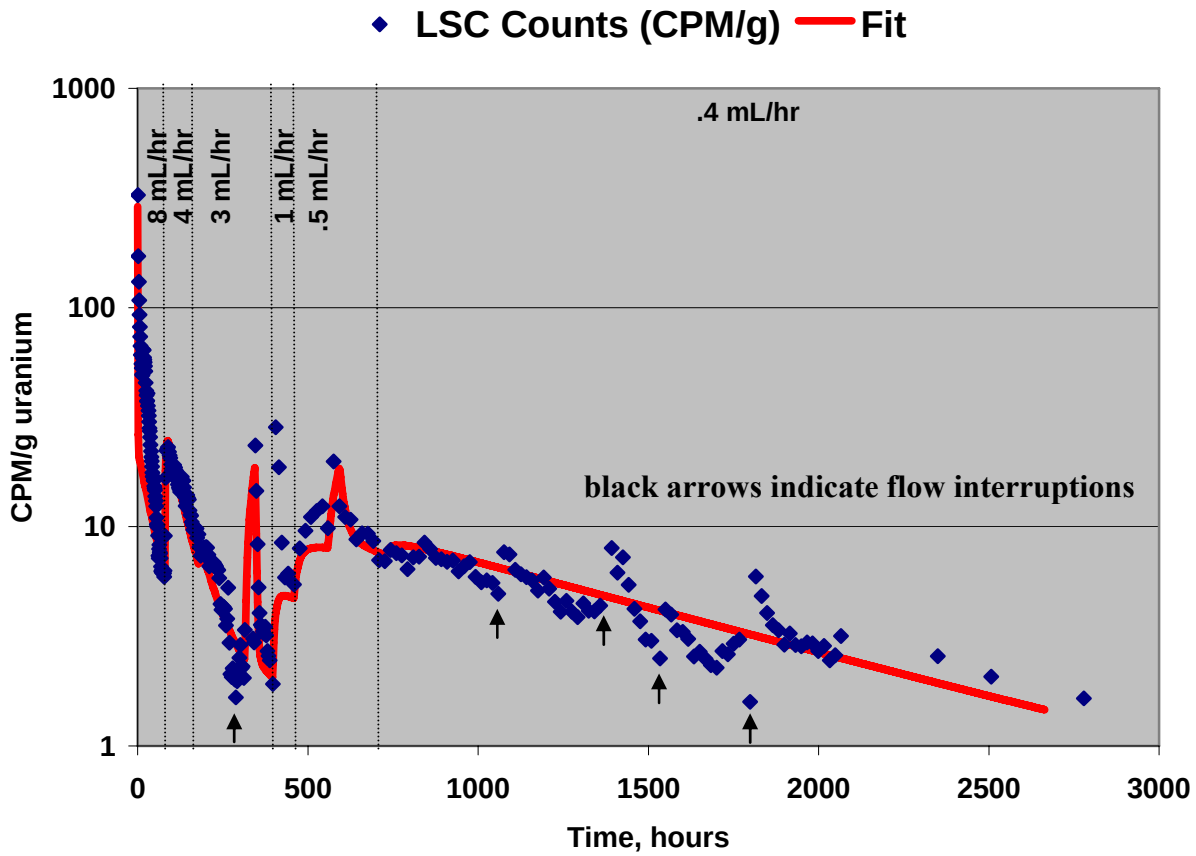

Figure 4.4. CPM/g Uranium Desorbed As A Function Of Time From 19IM1A Alluvium With 19D Zone 1 Groundwater. The fit of the data is obtained by using the uranium desorption model described in Section 3.1.2. The CPM/g of uranium desorbed over time was fit using a four-site desorption model with desorption rate constants ranging from .07 g/hr to .000001 g/hr. Note that this column run was for a period of approximately 3200 hours. Spikes in the CPM/g represent planned and un-planned flow interruptions and flow rate changes.

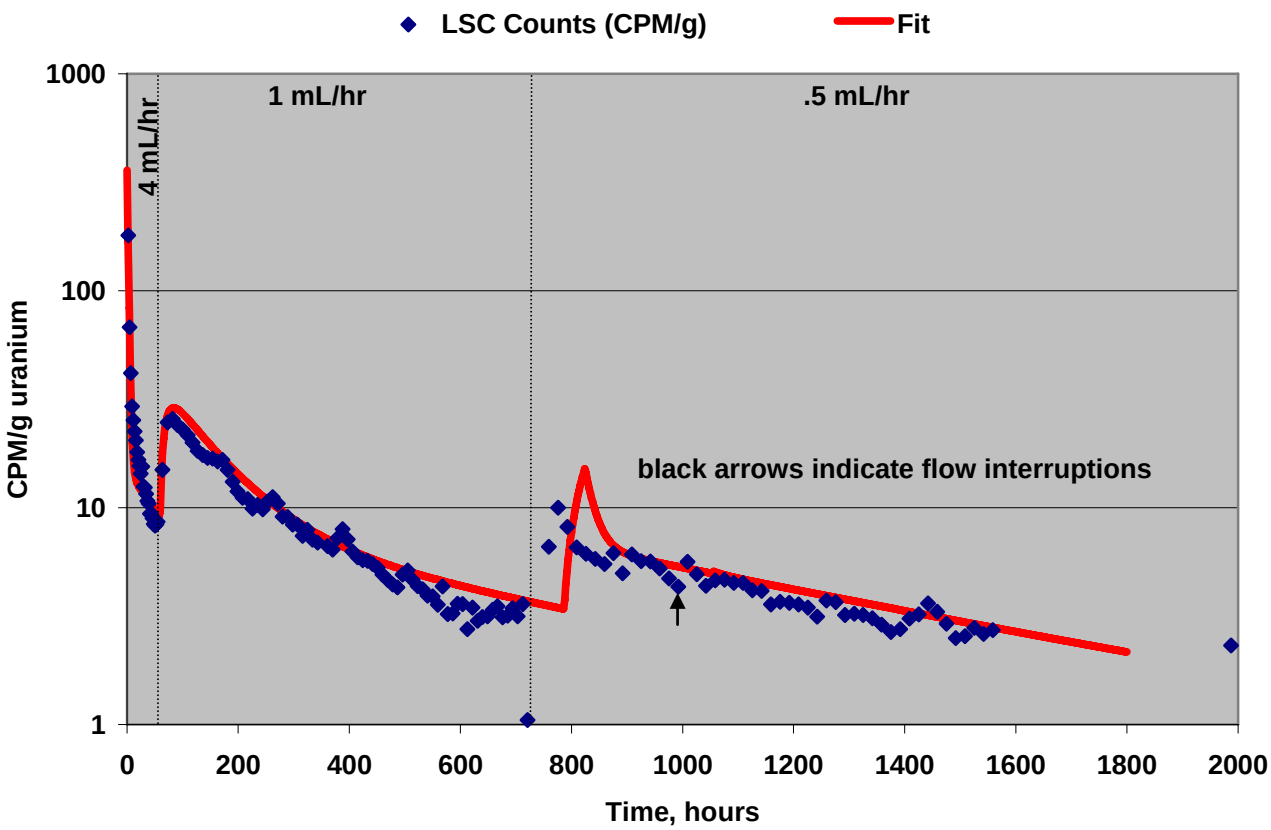

Figure 4.5. CPM/g Uranium Desorbed As A Function Of Time From 19IM1A Alluvium With 19D Zone 4 Groundwater. The fit of the data is obtained by using the uranium desorption model described in Section 3.1.2. The CPM/g of uranium desorbed over time was fit using a three-site desorption model with desorption rate constants ranging from .04 g/hr to .0001 g/hr. Note that this column run was for a period of approximately 2000 hours. Spikes in the CPM/g represent planned and un-planned flow interruptions and flow rate changes.

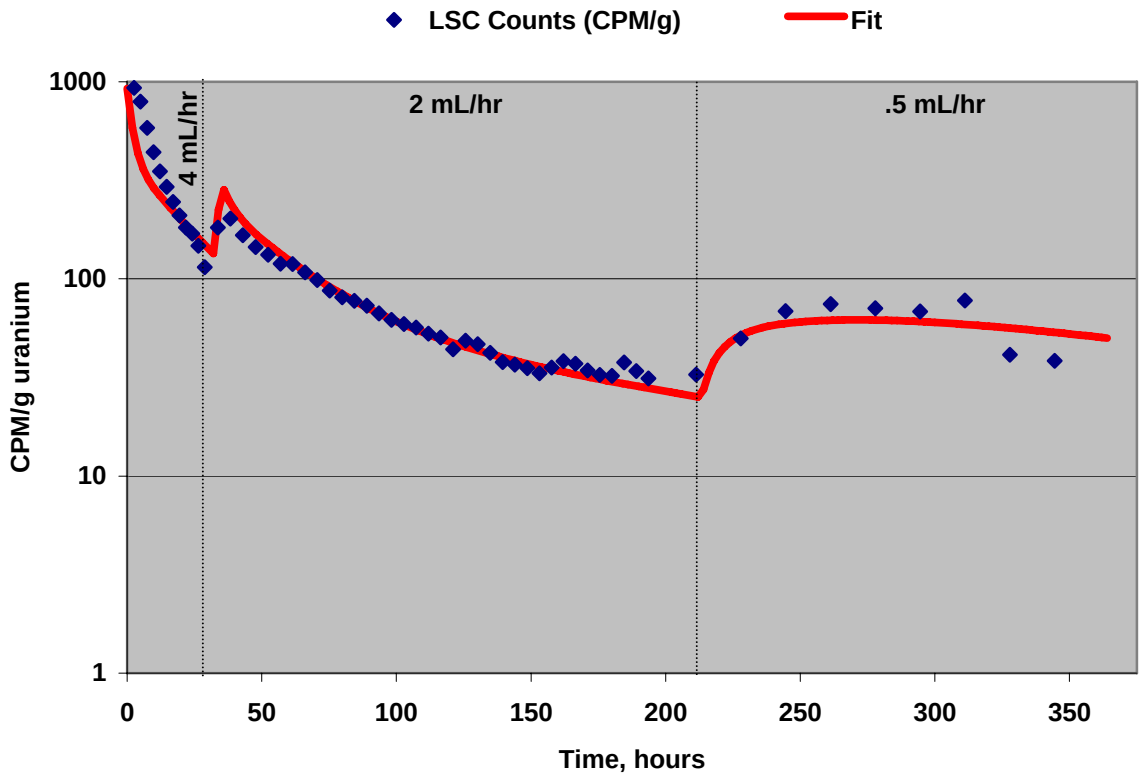

Figure 4.6. CPM/g Uranium Desorbed As A Function Of Time From 22SA Alluvium And With Zone 1 Groundwater. The fit of the data is obtained by using the uranium desorption model described in Section 3.1.2. The CPM/g of uranium desorbed over time was fit using a two-site desorption model with desorption rate constants ranging from .18 g/hr to .02 g/hr. Note that this column run was for a period of approximately 336 hours. Spikes in the CPM/g represent planned and un-planned flow interruptions and flow rate changes.

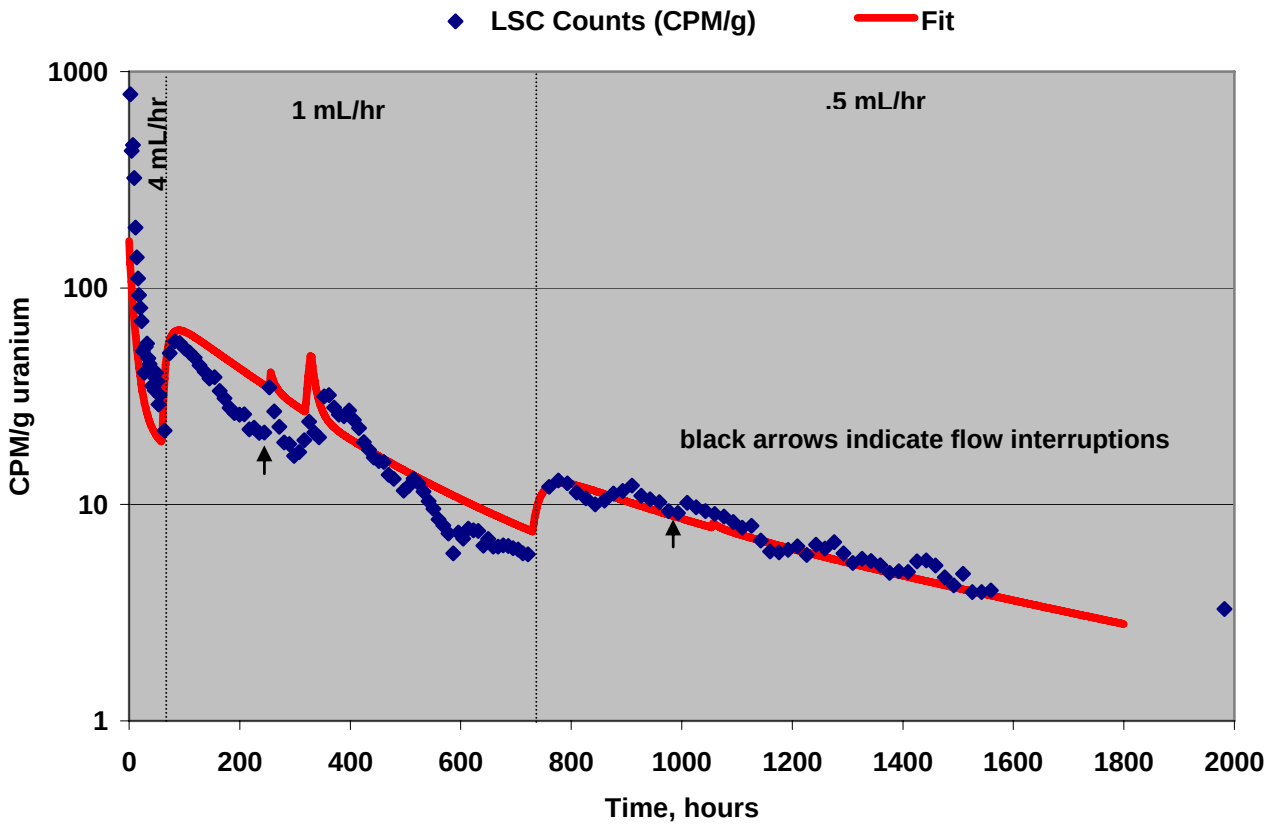

Figure 4.7. CPM/g Uranium Desorbed As A Function Of Time From 22SA Alluvium With 19D Zone 4 Groundwater. The fit of the data is obtained by using the uranium desorption model described in Section 3.1.2. The CPM/g of uranium desorbed over time was fit using a four-site desorption model with desorption rate constants ranging from .4 g/hr to .0001 g/hr. Note that this column run was for a period of approximately 2000 hours. Spikes in the CPM/g represent planned and un-planned flow interruptions and flow rate changes.

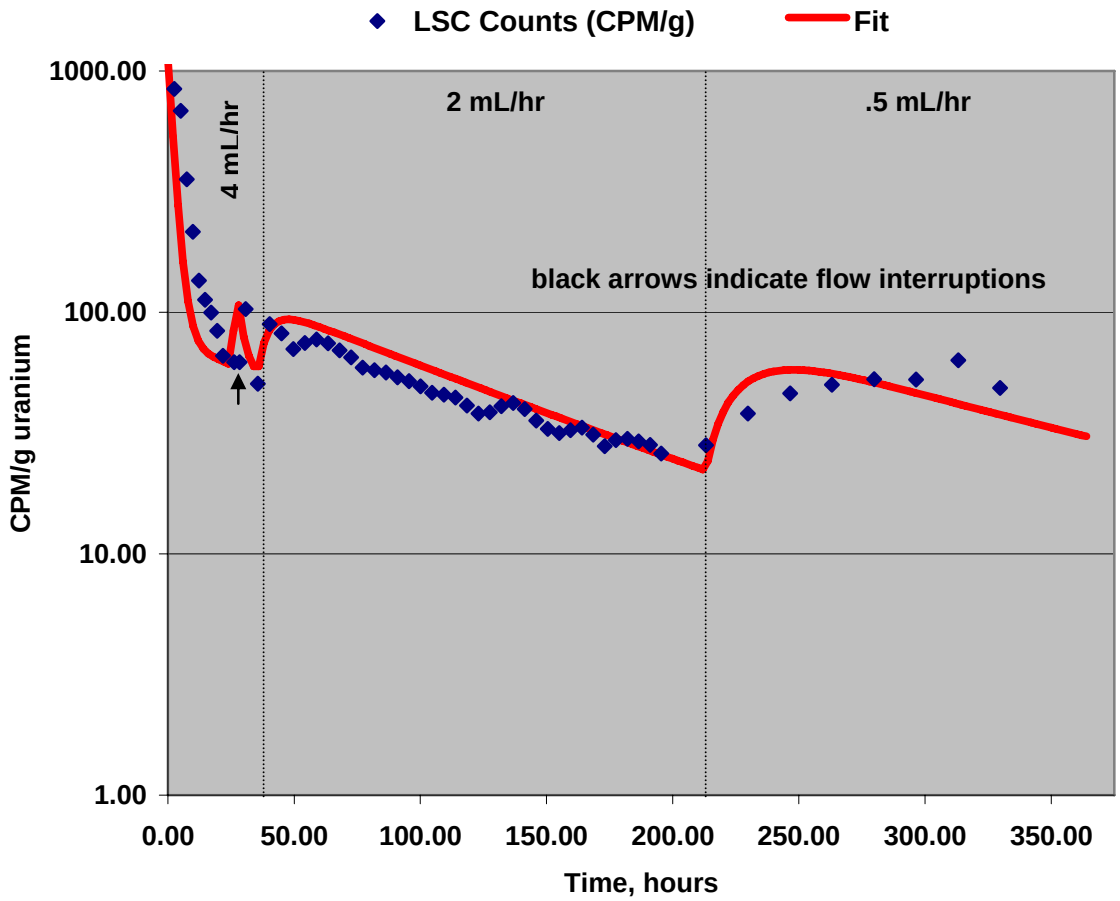

Figure 4.8. CPM/g Uranium Desorbed As A Function Of Time From 10SA Alluvium With 10SA Groundwater. The fit of the data is obtained by using the uranium desorption model described in Section 3.1.2. The CPM/g of uranium desorbed over time was fit using a two-site desorption model with desorption rate constants ranging from .04 g/hr to .0025 g/hr. Note that this column run was for a period of approximately 336 hours. Spikes in the CPM/g represent planned and un-planned flow interruptions and flow rate changes.

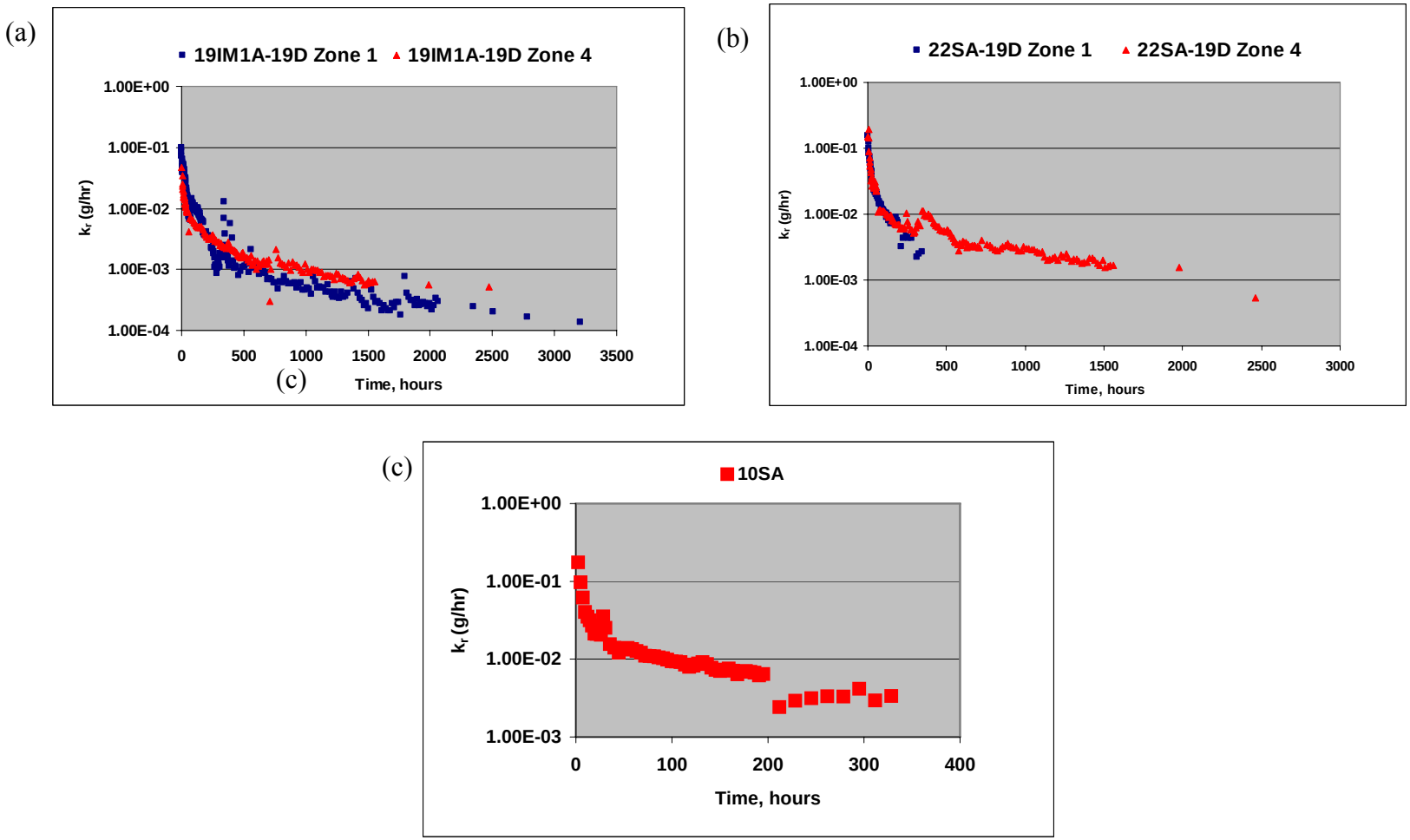

Figure 4.9. Uranium Desorption Rate Constants as a Function of Time for (a) 19IM1A alluvium with 19D Zone 1 and Zone 4 groundwater; (b) 22SA alluvium with 19D Zone 1 and Zone 4 groundwater; and (c) 10SA alluvium with 10SA groundwater. k_r is calculated using Equations 3.4 and 3.5 in Section 3.1.3.

4.5.2. Desorption rate constants, k_r

The data obtained from column desorption experiments (CPM/g uranium desorbed over time) were used to obtain the dC/dt for the use in Equation 3.5 described in Section 3.1.3. Continuous values of k_r were calculated over the entire uranium desorption period for each of the sample/groundwater combinations from one duplicate sample only. A semi-log plot of k_r vs. time is shown in Figure 4.9 (a), (b) and (c). Values of the desorption rate constant, k_r, range over two to three orders of magnitude depending on the length of the desorption. There is an apparent inconsistency between the ranges of rate constants for the finite number of reactions (Table 4.6) and the instantaneous rate constants calculated using equations 3.4 and 3.5 (Fig. 4.9). This inconsistency may be caused by the former approach accounting for multiple reactions occurring at any given point in time, whereas the latter approach simply assumes one reaction at each point in time. In any case, both methods support the existence of multiple desorption rate constants ranging over several orders of magnitude.

4.6. Electron Probe Microanalysis

Electron Probe Microanalysis (EPMA) was used to investigate the elemental associations of uranium sorbed to alluvial thin sections. False color maps and backscatter images are shown in Figures 4.10a through 4.14b. The false color maps show the intensity of each element using a color code that can be found to the right of each color map for each individual sample. Although the intensity levels vary between samples, the intensity increases from blue to red in the false color map for each element. Figure 4.10a is a false color map of the fine fraction (<75 μm) from

22SA Alluvium. The higher concentrations of uranium are indicated by the yellow and red pixels. The uranium appears to be spread evenly throughout the sample, making spot analysis selection difficult. Figure 4.10b is the backscatter image of the same particles; the numbers indicate the spot analysis locations. Spots 1-6 are below the detection limit for uranium. Analysis of spot 7 indicates that uranium is associated primarily with SiO_2 (46 wt.%), Al_2O_3 (15 wt.%) and FeO (7.5 wt.%). Figure 4.11a is from the middle size fraction (75 μm - 500 μm) of 22SA Alluvium. The concentrated green pixels on the uranium false color map were chosen for spot analysis. Analysis of spots 1, 2 and 4 shown on the backscatter image in Figure 4.11b indicate that uranium is associated primarily with SiO_2 and Al_2O_3. Figure 4.12a is from the coarse fraction (500 μm - 2000 μm) of 22SA Alluvium. The uranium false color map indicates that this element can only be found in one area associated with small particles surrounded by carbon. The alluvial thin sections were prepared using an epoxy resin to affix particles. The epoxy resin appears black in the backscatter image (Figure 4.12b). Although uranium is above the detection limit at spot 1, analysis indicates an overwhelming mass percent of carbon most likely a result of the surrounding epoxy resin. Spots 2 through 4 are also above the detection limit for uranium, although wavelength dispersive x-ray spectrometer (WDS) analysis resulted in low mass percents for other analytes and uranium-mineral associations could not be determined. Figure 4.13a is also from the coarse fraction of 22SA Alluvium and represents a single mineral grain. The grain appears to be primarily composed of Si and Al with an Fe vein running across the surface and along the top edge. Uranium is concentrated along the top edge with smaller amounts associated with the Fe vein.

Analyses of spots 1, 3, 4, 5, 6, and 8 shown in Figure 4.13b indicate that uranium is associated with FeO (42 to 89 wt.%) as well as SiO_2 and Al_2O_3. The uranium found at spot 7 is primarily associated with SiO_2 and Al_2O_3, with only 2 mass percent FeO. Matrix analyses at spots 9 and 10 (no U association) indicate that the specimen is a coarse clay particle. Although spot 11 is 77 mass percent FeO, uranium is not found at this location. The uranium association with iron is apparent in the false color map shown in Figure 4.14a, which is from the medium fraction (75 μm - 500 μm) of 19IM1A Alluvium. The object in the backscatter image (Figure 4.14b) appears to be something other than a mineral grain. Analyses of spots 1-7 indicate uranium levels above the detection limit. Overwhelmingly high intensity iron is found at Spots 1 and 4 (believed to be elemental Fe) and the remaining spots contain high mass percents of iron oxide, suggesting that this object may be sample contamination. However, the results support the correlation between uranium and iron oxide coatings on minerals. Detailed results for each sample are shown in Appendix 6, along with the detection limit for each element contained in Appendix 7.

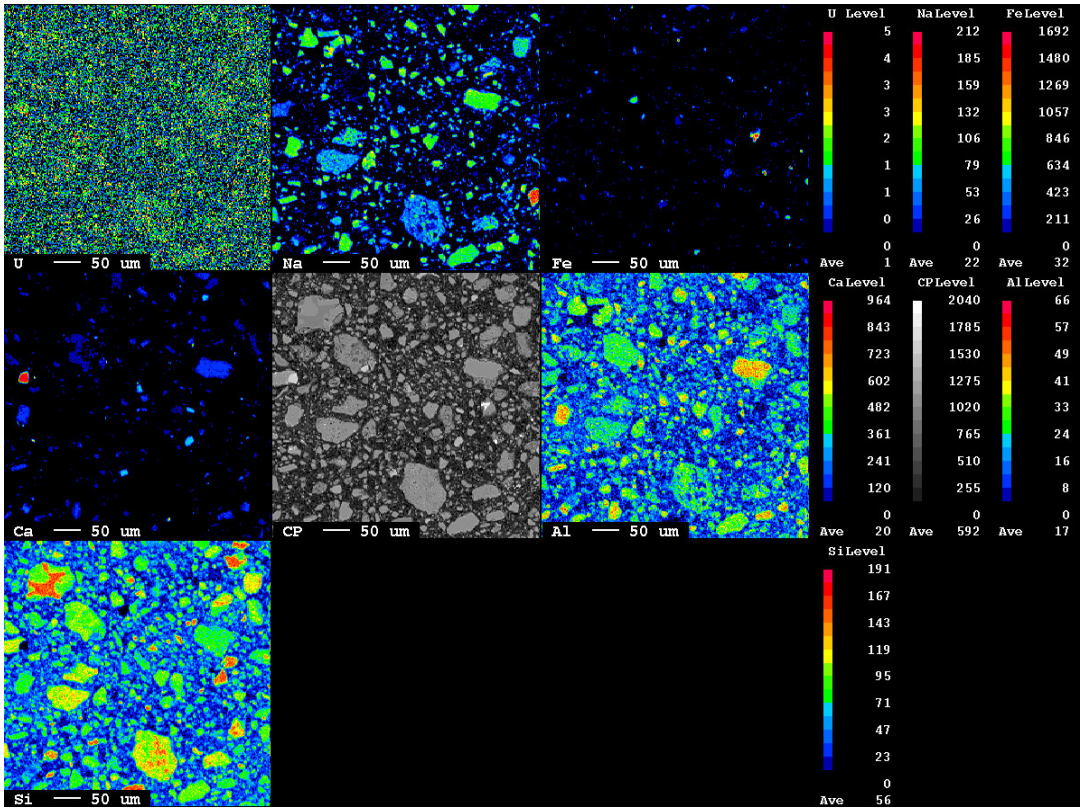

Figure 4.10a. EPMA False Color Map of Fine Fraction from 22SA Alluvium. False color maps for Uranium (U), Sodium (Na), Iron (Fe), Calcium (Ca), Aluminum (Al) and Silicon (Si) show intensity correlations between the elements. Element intensity increases from blue to red.

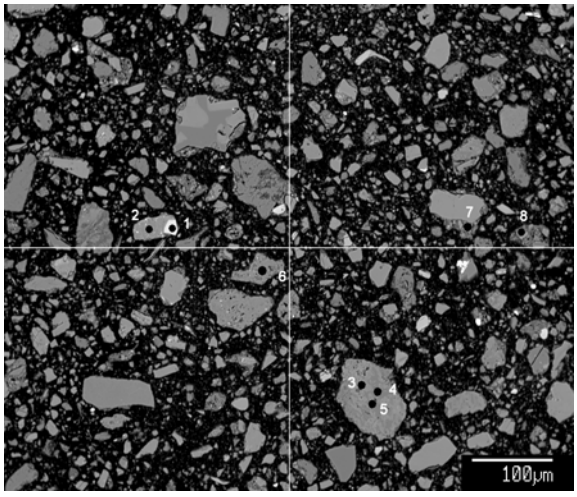

Figure 4.10b. EPMA Backscatter Image of Fine Fraction from 22SA Alluvium. High intensity areas (red pixels) of the uranium false color map are chosen for WDS spot analysis. Spots 1-6 are below the detection limit for uranium. Analysis of spot 7 indicates that uranium is associated primarily with SiO_2 (46 wt.%), Al_2O_3 (15 wt.%) and FeO (7.5 wt.%).

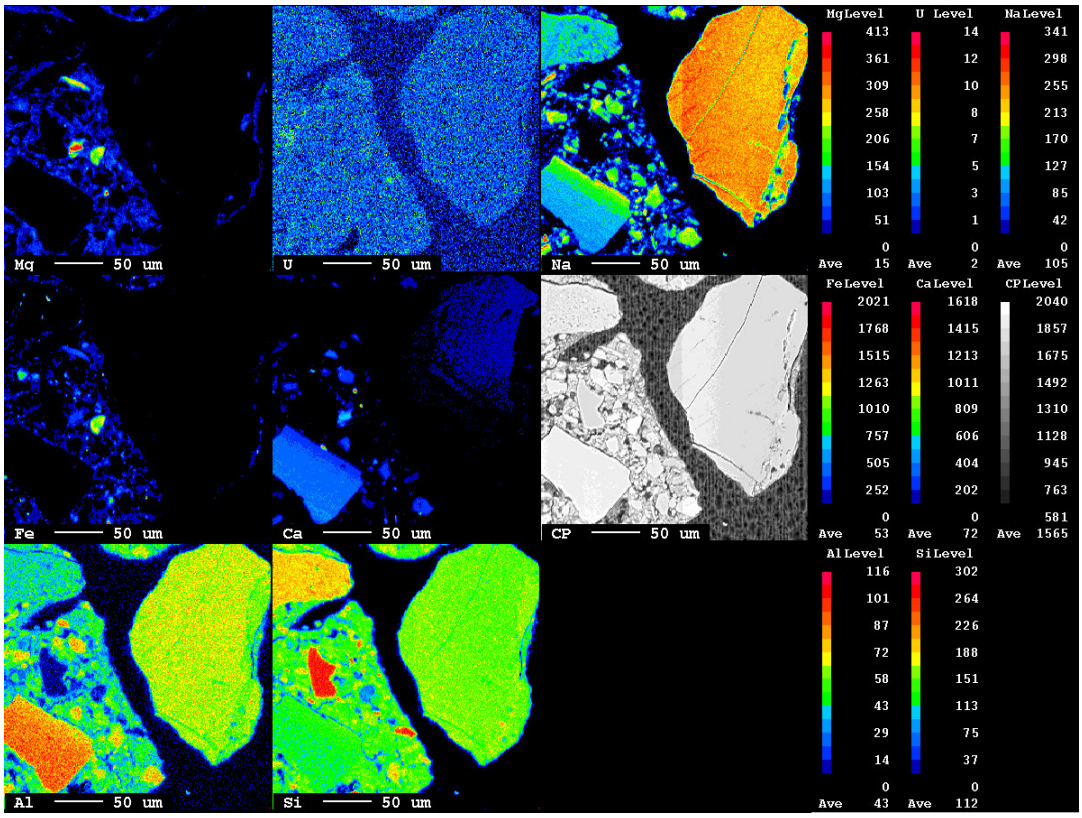

Figure 4.11a. EPMA False Color Map of Medium Fraction from 22SA Alluvium. False color maps for Magnesium (Mg), Uranium (U), Sodium (Na), Iron (Fe), Calcium (Ca), Aluminum (Al) and Silicon (Si) show intensity correlations between the elements.

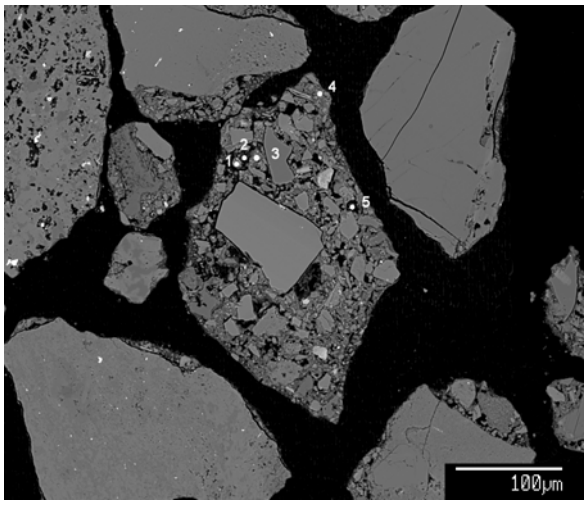

Figure 4.11b. EPMA Backscatter Image of Medium Fraction from 22SA Alluvium. Spot 3 is below the detection limit for uranium. Analysis of spots 1, 2 and 4 indicate that uranium is associated primarily with SiO_2 and Al_2O_3. No data are available for spot 5.

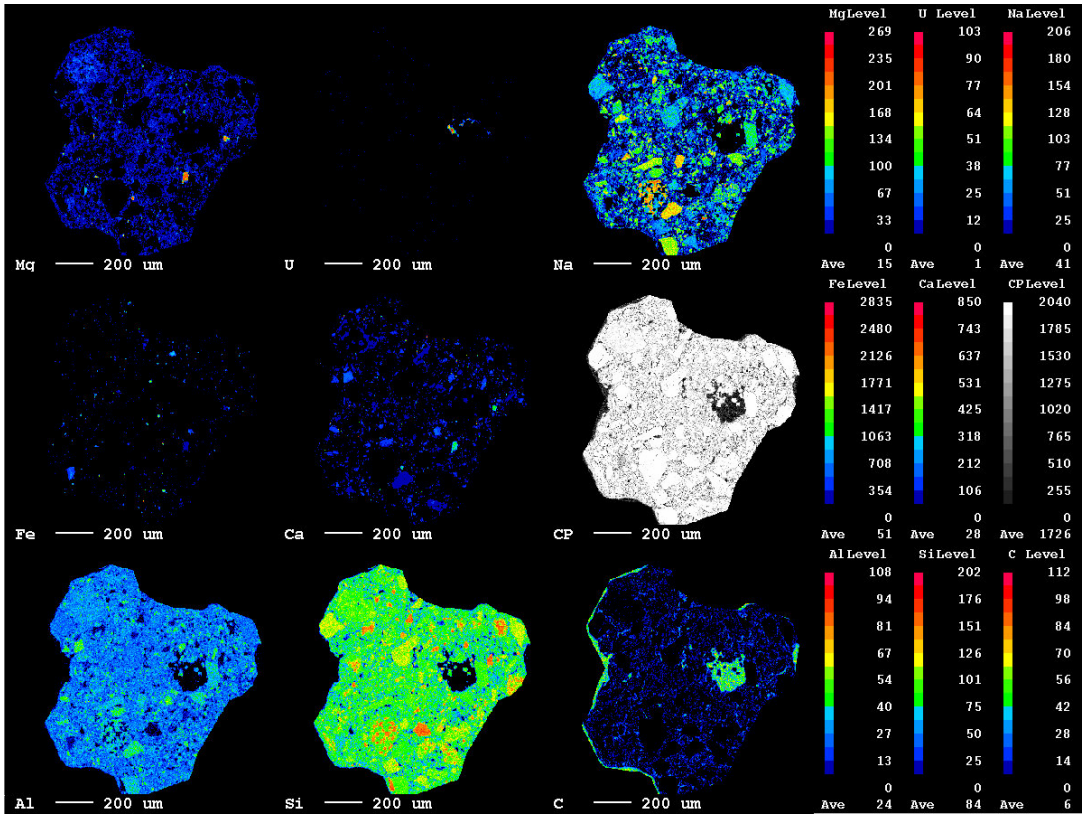

Figure 4.12a. EPMA False Color Map of Coarse Fraction from 22SA Alluvium. False color maps for Magnesium (Mg), Uranium (U), Sodium (Na), Iron (Fe), Calcium (Ca), Aluminum (Al), Silicon (Si) and Carbon (C) show intensity correlations between the elements. Carbon intensities are primarily due to the epoxy resin used in the thin section preparation. From the false color map, uranium appears to be associated primarily with Si and Al.

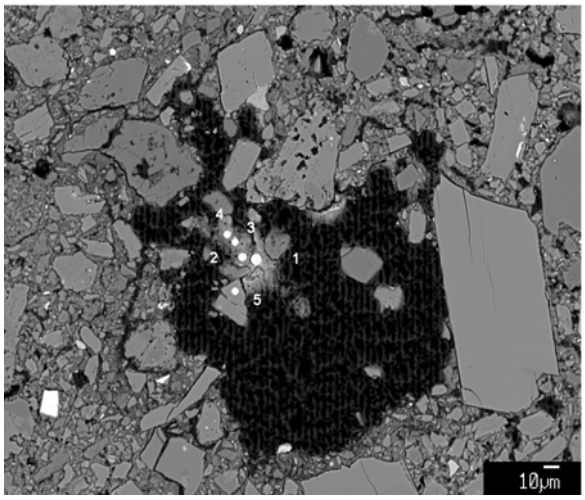

Figure 4.12b. EPMA Backscatter Image of Coarse Fraction from 22SA Alluvium. The epoxy resin appears black in this backscatter image. Although uranium is above the detection limit at spot 1, analysis indicates an overwhelming mass percent of carbon most likely a result of the surrounding epoxy resin. Spots 2 through 4 are also above the detection limit for uranium, although WDS analysis for associated elements is inconclusive.

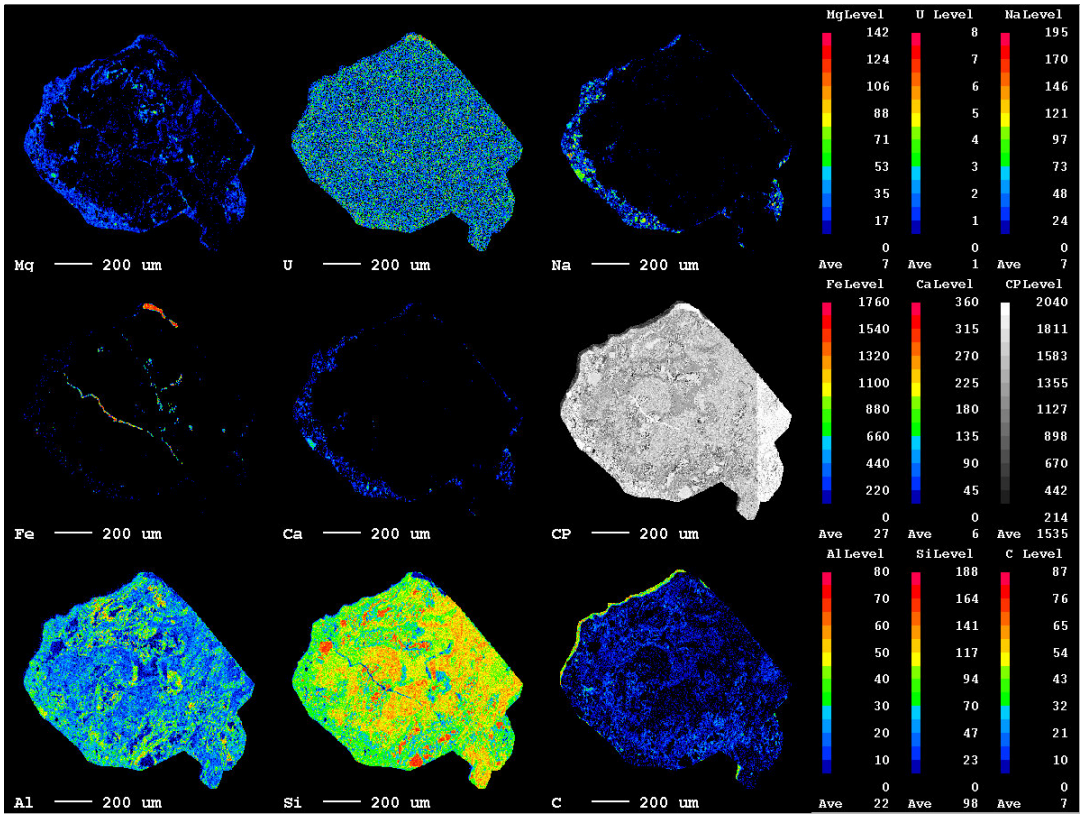

Figure 4.13a. EPMA False Color Map of Coarse Clay Particle from 22SA Alluvium. False color maps for Magnesium (Mg), Uranium (U), Sodium (Na), Iron (Fe), Calcium (Ca), Aluminum (Al), Silicon (Si) and Carbon (C) show intensity correlations between the elements. The grain appears to be primarily composed of Si and Al with an Fe vein running across the surface and along the top edge. Uranium appears to be concentrated along the top edge with smaller amounts associated with the Fe vein.

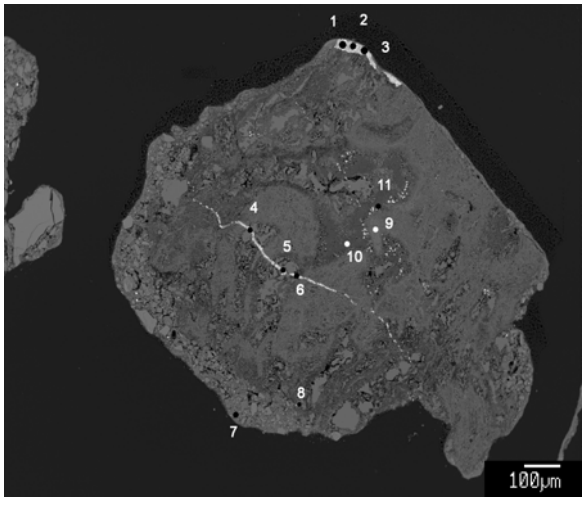

Figure 4.13b. EPMA Backscatter Image of Coarse Clay Particle from 22SA Alluvium. Analyses of spots 1, 3, 4, 5, 6, and 8 indicate that uranium is associated with FeO (42 to 89 wt.%) as well as SiO_2 and Al_2O_3. Uranium is below the detection limit at spot 2. Uranium found at spot 7 is primarily associated with SiO_2 and Al_2O_3, with only 2 mass percent FeO. Matrix analyses at spots 9 and 10 (no U association) indicate that the specimen is a coarse clay particle. Although spot 11 is 77 mass percent FeO, uranium is not found at this location.

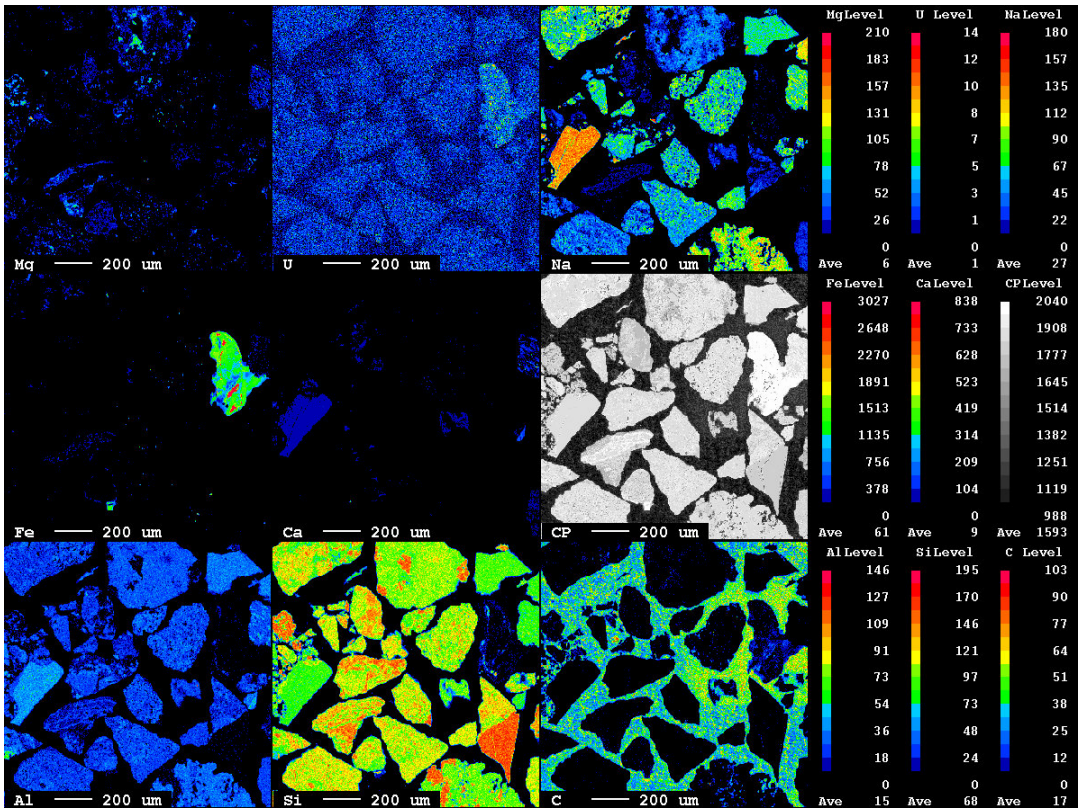

Figure 4.14a. EPMA False Color Map of Medium Fraction from 19IM1A Alluvium. False color maps for Magnesium (Mg), Uranium (U), Sodium (Na), Iron (Fe), Calcium (Ca), Aluminum (Al), Silicon (Si) and Carbon (C) show intensity correlations between the elements. Uranium is clearly associated with the high intensity iron found in the Fe false color map.

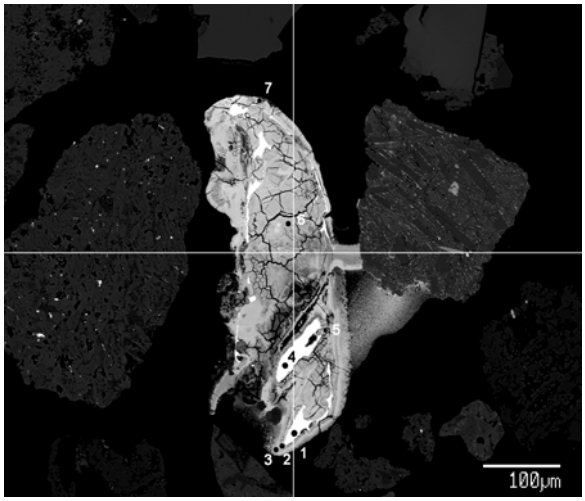

Figure 4.14b. EPMA Backscatter Image of Medium Fraction from 19IM1A Alluvium. The object in the backscatter image appears to be something other than a mineral grain. Analyses of Spots 1-7 indicate uranium levels above the detection limit. Overwhelmingly high intensity iron is found at Spots 1 and 4 (believed to be elemental Fe) and the remaining spots contain high mass percents of iron oxide, suggesting that this object may be sample contamination. However, the object (whether natural to the alluvium or not) supports the correlation between uranium and iron oxide coatings on minerals.

5. DISCUSSION

5.1. Adsorption and Desorption Rates of Uranium in Alluvium

The symmetric break through curve and near complete recovery of the conservative tracer in the continuous flow column experiments (Figures 1.2, 1.3 and 1.4) do not indicate preferential flow paths and dead volume as a factor in the observed uranium breakthrough behavior. Therefore, the observed uranium breakthrough behavior in these experiments suggests that some of the uranium was slow to desorb from the column material. In addition, the predicted uranium breakthrough curves based on batch K_d values suggest a much later (up to 10 times later) breakthrough of uranium than observed in the columns. Column transport predictions using K_d values to represent sorption are based on the assumption of local equilibrium although, given the conflicting results between batch and column experiments, this may not be the case. The purpose of the flow-through desorption columns designed for this study is to achieve "well-mixed" conditions (no concentration gradients) within the column. This has been done to measure in detail the desorption rates of uranium from mineral surfaces, eliminating other factors that may affect uranium transport.

The results of the uranium desorption study suggest that there are multiple types of sites for uranium sorption reactions with varying desorption kinetics. Possible mechanisms for uranium sorption exist and may include ionic bonding with negatively charged clay surfaces (electrostatic adsorption), surface complexation reactions (chemical adsorption), and precipitation reactions. Given the chemistry of

the systems in this study, precipitation reactions can most likely be ruled out as a possible mechanism of uranium removal from solution.

5.2. Parameter Effects on Sorption and Desorption of Uranium

5.2.1. Effects of Water Chemistry on Uranium Speciation and Sorption

It would appear from Figures 4.1, 4.2 and 4.3 that water chemistry parameters play an important role in the behavior of uranium tracer solution in contact with the alluvium samples in this study. The batch sorption of uranium using 19D Zone 1 groundwater results in greater partitioning of uranium to the solid phase for both the 19IM1A and 22SA alluvium when compared to the experiments performed with the 19D Zone 4 groundwater. This is most likely due to the higher amount of negatively charged and un-charged uranyl carbonate species formed in the higher carbonate water (Zone 4). The carbonate species that dominate for a solution of uranium in pure H_2O at atmospheric conditions and the pH range of the groundwater in this study are $UO_2(CO_3)_2^{2-}$ and $UO_2(CO_3)_3^{4-}$ (Langmuir 1997). To support this argument, the results of PHREEQC calculations showing the predicted uranium solution speciation in the different waters are presented in Table 5.1. The $UO_2(CO_3)_2^{2-}$ and $UO_2(CO_3)_3^{4-}$ species concentrations are 2-10 orders of magnitude greater than the other uranium species in solution for each groundwater. These complexes are negatively charged and the uranium would therefore not readily adsorb by ion exchange or an electrostatic process to a negatively charged clay mineral surface. Desorption of uranium also appears to be dependent on water chemistry and the amount of uranium initially sorbed on the alluvium. In each case, the greater the

initial uranium sorption, the greater the amount of uranium from the initial amount in contact with the alluvium remains sorbed at the end of the desorption period. As pH increases, the amount of uranyl carbonate species increases and therefore there is also an indirect negative correlation of uranium sorption and desorption on the pH of the solution.

Table 5.1. Speciation of a 10^{-6}M U(VI) tracer solution in groundwater calculated by PHREEQC

	Dominant Form of U(6)	Concentration (m)	Second Most Abundant Form of U(6)	Concentration (m)
Well NC-EWDP-19D Zone 1	$UO_2(CO_3)_3^{4-}$	5.063e-07	$UO_2(CO_3)_2^{2-}$	4.913e-07
Well NC-EWDP-19D Zone 4	$UO_2(CO_3)_3^{4-}$	6.504e-07	$UO_2(CO_3)_2^{2-}$	3.489e-07
Well NC-EWDP-10SA	$UO_2(CO_3)_2^{2-}$	5.884e-07	$UO_2(CO_3)_3^{4-}$	4.073e-07

It is difficult to deduce from this study the dependence of uranium sorption and desorption on the ionic strength of the groundwater. The 10SA groundwater has the lowest ionic strength but was not used in experiments other than that of the 10SA alluvium. Given that the mineralogy of the three alluviums differ, it is difficult to compare the effects of ionic strength between the samples.

It is interesting to note that the 22SA column desorption experiments performed with 19D Zone 4 water result in greater uranium desorption than the 19IM1A 19D Zone 4 experiments, although the initial amount sorbed in the 22SA experiments was greater (Figure 4.3 a. and b.). This behavior was not seen in the step-wise batch desorption results in Figure 4.2 where the alluvium was in contact

with the same tracer free groundwater for a week at each step. This may suggest a possible mechanism present in the 22SA alluvium system on which desorption is more dependent on uranyl carbonate complex formation and uranium solution concentration than that of the 19IM1A system. In other words, in the batch desorption the alluvium is in contact with the same solution for one week for each time step until the supernatant is removed and replaced with fresh tracer-free groundwater. It is assumed in this situation that uranium is being desorbed and re-sorbed throughout the duration of the step. In the column desorption, the tracer-free groundwater is being continuously circulated through the alluvium and re-sorption of the uranium has less time to take place.

5.2.2. Mineralogical Effects on Uranium Sorption

Major and trace mineralogy, as well as surface area appear to play an important role in the sorption of uranium to alluvium used in the study. The alluvium from 22SA consistently results in higher sorption of uranium when compared to 19IM1A in both the 19D Zone 1 and 19D Zone 4 groundwater and is greater than 10S when the 19D Zone 1 groundwater is used. The weight percent of clay minerals (smectite) and surface area of the 22SA alluvium is greater than that of both the 19IM1A and 10SA alluvium. The results of the iron oxide extractions appear to have a positive correlation with the amount of clay minerals in alluvium and may also have an effect on sorption of uranium.

5.3. Electron Probe Microanalysis

Although uranium-mineral associations cannot be fully quantified using EPMA data, this analysis tool allows the user to see first hand the elements with

which uranium is associated. EPMA is an effective tool when accompanying other types of analysis such as Quantitative X-ray Diffraction (QXRD) to determine the mineral phases present in geologic samples. The EPMA results presented in this thesis suggest that uranium is associated with aluminum, silicon and iron oxide. This information along with the QXRD results for these samples (provided in Table 4.4) suggests that uranium is most likely associated with clay minerals and iron oxide coatings on minerals. These conclusions are based on the high mass percent of clay present in the sample and very low mass percent of iron (hematite) found in QXRD analysis. The low mass percent of crystalline iron phases suggests that the high mass percent of iron found in the EPMA was found largely as amorphous iron oxide, not analyzed with QXRD analysis.

EPMA used to study the elemental associations of uranium in the alluvium supports the theory of multiple sorption sites, although further analysis of the system such as measurement of uranium speciation both in solution and sorbed on the surface is needed to fully understand sorption mechanisms.

5.4. Implications for Large-Scale Predictive Modeling and Remediation

The current approach to modeling radionuclide transport in the saturated alluvium at Yucca Mountain considers only single K_d values for the partitioning of uranium between the solution and solid phases. It does not consider sorption onto multiple types of sites present in the alluvium, or take into account variations in water chemistry. It also assumes that sorption of radionuclides to matrix material is fast and completely reversible (described by a K_d modeling approach). It is quite likely that radionuclide transport rates in the saturated zone may be over-predicted by using a K_d

approach. The experiments and modeling conducted in this study are intended to relax much of this conservatism and to provide a sound basis for making more realistic predictions of radionuclide transport rates in the saturated zone.

6. CONCLUSIONS AND FUTURE WORK

The extent to which uranium will migrate from a high level nuclear waste repository depends on the ability of engineered barriers and natural systems to retard the migration of uranium. Migration of uranium in the saturated zone depends ultimately on two major factors: (1) The rate and direction of groundwater flow and (2) the ability of the host rock materials to adsorb uranium. This study focuses on the second factor, the ability of the saturated alluvium to retard the migration of uranium.

It is overly simplistic to explain the sorption of uranium in a heterogeneous media by a single partition coefficient. Variability in desorption rates are not always considered, but they may ultimately control uranium transport behavior. This is important because risk and performance assessments are concerned with the transport of contaminants over years to thousands of years, not just a few weeks. (Kaplan et al. 1998).

Further study is required to increase our understanding of the behavior of uranium in the saturated alluvium at Yucca Mountain. A proposal for future work would include:

- Investigation of the uranium desorption dependence on contact time with alluvium during the initial sorption phase to assess the probability of sorption to “strong sites” at different contact times;

- Investigation of the uranium desorption dependence on pH, ionic strength and carbonate concentration to aid in the understanding of the mechanisms of uranium sorption and desorption in alluvium;
- Investigation of the existence of a positive correlation of uranium sorption with oxyhydroxide species.
- Utilization of Transmission Electron Microscopy (TEM) analysis to determine atomic level associations of uranium-sorbed alluvium samples.
- Determination of the oxidation state of uranium in solution pre and post contact with alluvium using spectroscopic studies to aid in the understanding of chemical mechanisms of uranium sorption and desorption in alluvium (i.e., perhaps the "strongly" sorbed U is reduced, whereas the more weakly sorbed U is still U(VI));
- Investigation of the groundwater flow behavior and in situ transport behavior of reactive species through column transport studies to understand how the observations of widely varying desorption rates translate to dynamic transport behavior under flowing conditions.

The results of the current study and the proposed future work can be used to improve models for transport and fate of uranium at Yucca Mountain. The understanding of the desorption behavior of uranium in heterogeneous systems would result in less conservative performance assessment models than those based solely on K_d values. Other benefits include the ability to predict uranium transport behavior in other heterogeneous systems based on bulk mineralogy and water chemistry information with a decreased need for extensive sorption and desorption experiments.

In addition, the increased understanding of the governing mechanisms of uranium transport would increase confidence in laboratory studies to accurately describe field transport behavior. This field of research can potentially have application in homeland defense, groundwater quality issues and environmental remediation.

REFERENCES

Barnett, M. O., P. M. Jardine, et al. (2000). "Adsorption and transport of uranium(VI) in subsurface media." Soil Science Society of America Journal **64**(3): 908.

Brunauer, S. E., P. H.; Teller, E. (1938). "Adsorption of gases in multimolecular layers." J. Am. Chem. Soc., vol. 60, p. 309-319 (1938). **60**: 309-319.

Chipera, S. J. and D. L. Bish (2002). "FULLPAT: a full-pattern quantitative analysis program for X-ray powder diffraction using measured and calculated patterns." Journal of Applied Crystallography **35**: 744.

Davis, J. A. and D. B. Kent (1990). "SURFACE COMPLEXATION MODELING IN AQUEOUS GEOCHEMISTRY." Reviews in Mineralogy **23**: 177.

Drever, J. I. (1997). The Geochemistry of Natural Waters. Upper Saddle River, Prentice Hall, 436.

Echevarria, G., M. I. Sheppard, et al. (2001). "Effect of pH on the sorption of uranium in soils." Journal of Environmental Radioactivity **53**(2): 257.

Eddebbarh, A. A., G. A. Zyvoloski, et al. (2003). "The saturated zone at Yucca Mountain: An overview of the characterization and assessment of the saturated zone as a barrier to potential radionuclide migration." Journal of Contaminant Hydrology **62-63**: 477.

EPA (1996). Test methods for evaluating solid waste physical/chemical methods (SW-846) {electronic resource} Method 6010B Inductively Coupled Plasma-Atomic Emission Spectrometry (ICP-AES). O. o. S. Waste, U.S. Environmental Protection Agency, Office of Solid Waste **2005**.

Francis, A. J. (1998). "Biotransformation of uranium and other actinides in radioactive wastes." Journal of Alloys and Compounds **271-273**(0): 78-84.

Gabriel, U., J. P. Gaudet, et al. (1998). "Reactive transport of uranyl in a goethite column: an experimental and modeling study." Chemical Geology **151**(1-4): 107.

Hsi, C. D. C.-K. (1981). Sorption of uranium (VI) by iron oxides

Hsi, C. K. D. and D. Langmuir (1985). "Adsorption Of Uranyl Onto Ferric Oxyhydroxides - Application Of The Surface Complexation Site-Binding Model." Geochimica et Cosmochimica Acta **49**(9): 1931.

Kaplan, D. I., T. L. Gervais, et al. (1998). "Uranium(VI) sorption to sediments under high pH and ionic strength conditions." Radiochimica Acta **80**(4): 201.

Langmuir, D. (1997). Aqueous environmental geochemistry. Upper Saddle River, N.J., Prentice Hall, c1997600.

Lenhart, J. J. and B. D. Honeyman (1999). "Uranium(VI) sorption to hematite in the presence of humic acid." Geochimica et Cosmochimica Acta **63**(19-20): 2891.

Loeppert, R. H. and W. P. Inskeep (1996). Iron Methods in Soil Analysis, Part 3. Madison, SSSA and ASA639-664.

Morris, D. E. (2002). "Redox energetics and kinetics of uranyl coordination complexes in aqueous solution." Inorganic Chemistry **41**(13): 3542.

Nye County Nuclear Waste Repository Program Office Early Warning Drilling Program, http://www.nyecounty.com/ewdpmain.htm, 2005

Prikryl, J. D., R. T. Pabalan, et al. (1994). "Uranium sorption on alpha-alumina: Effects of pH and surface-area solution-volume ratio." Radiochimica Acta **66-7**: 291.

Reimus, P. W., M. Ding, et al. (2005). OSTI 3rd Quarter Progress Report for FY 2005: Improved Characterization of Radionuclide Retardation in Volcanics and Alluvium. Los Alamos, New Mexico, Los Alamos National Lab**:** 5.

Schweich, D. and M. Sardin (1981). "Adsorption, Partition, Ion Exchange And Chemical Reaction In Batch Reactors Or In Column--A Review." J Hydrol **50**(1-3): 1.

Stammose, D., J. Ly, et al. (1992). "Sorption mechanisms of three actinides on a clayey mineral." Applied Clay Science **7**(1-3): 225-238.

Stewart, C. L., L. J. Reimann, et al. (2000). Mineralogic considerations for uranium in-situ leach mining: A Preliminary study of uranium and associated mineralogy of roll-front uranium deposits in Wyoming and Nebraska. 30th Annual Hydrometallurgical Conference; September 9-15, 2000; Saskatoon, Canada, Saskatoon, Canada, Canadian Inst Mining, Metallurgy And Petroleum.

Stumm, W. (1992). Chemistry of the Solid-Water Interface, John Wiley & Sons, Inc.

Waite, T. D., J. A. Davis, et al. (1994). "Uranium(Vi) Adsorption To Ferrihydrite - Application Of A Surface Complexation Model." Geochimica et Cosmochimica Acta **58**(24): 5465.

APPENDICES

APPENDIX 1-Well Location Maps & Projected Flow Paths

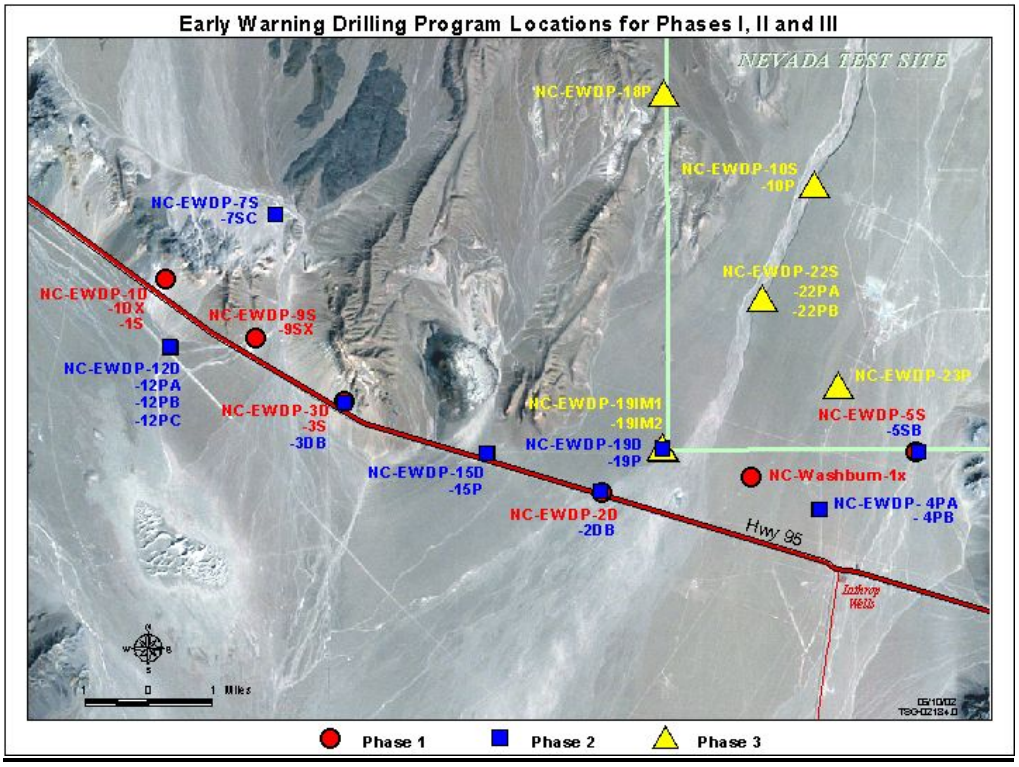

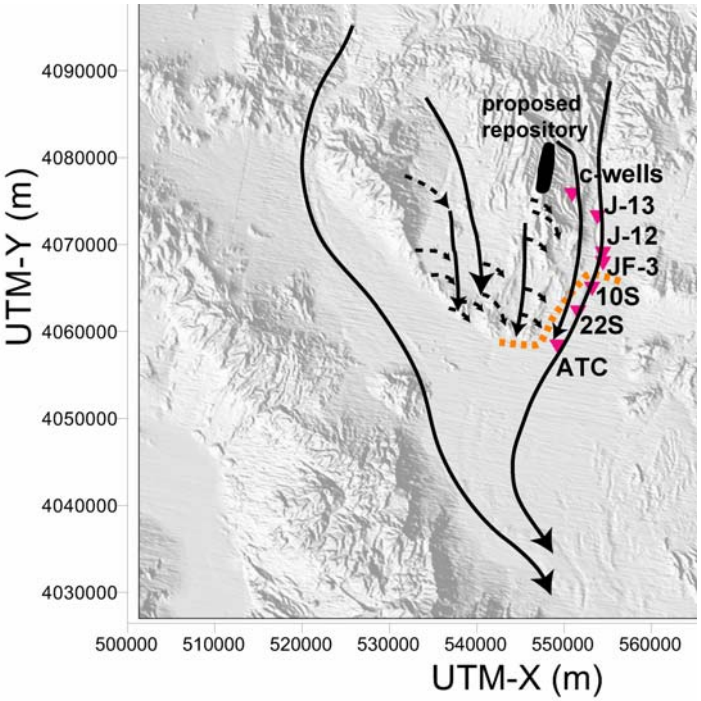

Groundwater flow is generally to the south and east of the proposed repository. The water table transitions from volcanics to alluvium in Fortymile Wash (orange-dashed line). NC-EWDP-19IM1A is located in the Alluvial Testing Complex (ATC).

APPENDIX 2A-19IM2A Summary Lithology Log

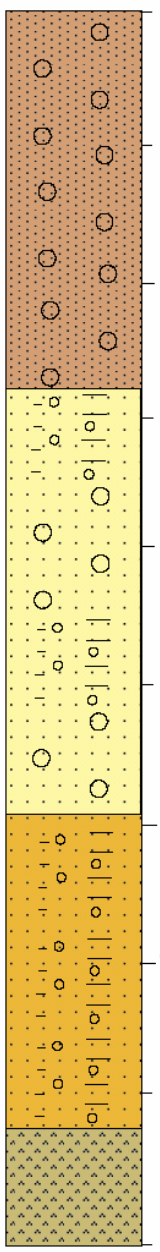

0 to 280 ft WELL-GRADED SAND with silt and gravel (SW-SM)

SW-SM layers up to 60 ft thick predominate. Numerous thin (10 or more) well-graded sand with gravel layers (SW) up to 15 ft thick are present in the upper 225 ft. Less numerous well-graded gravels with silt layers (GW-GM) predominantly less than 5 ft thick are present in the upper 250 ft. Several widely spaced layers of silty sand with gravels (SM) less than 5 ft thick are present below 200 ft. Fines in the SM layers are non-plastic. Samples exhibited weak cementation from 0 to 70 ft and 102.5 to 112.5 ft. Gravel clasts are volcanic in origin and are subangular to subrounded. Sediment color ranges from moderate yellowish brown (10YR 5/4) to dark yellowish brown (10YR 4/2). A strong reaction to 10% HCl is displayed in sediments from 0 to 50 ft; moderate reaction from 50 to 70 ft and 102.5 to 112.5 ft; and no reaction in the remaining sediments. All samples were dry.

280 to 595 ft ALTERNATING WELL-GRADED SAND with silt and gravel (SW-SM) and SILTY SAND with gravel (SM)*

Overall proportion of SW-SM and SM layers are approximately equal with SM layers becoming more frequent with depth. A thin well-graded gravel layer (GW) is present from 560 to 565 ft. Fines in SM layers are predominantly non-plastic with minor occurrence of low plasticity. Gravel clasts are predominantly volcanic in origin and range from subangular to subrounded. Sediment color ranges from moderate yellowish brown (10YR 4/4) to dark yellowish brown (10YR 4/2). No cementation was observed except a weakly cemented zone from 362 to 390 ft. No reaction to 10% HCl was observed. Samples were dry to 362 ft, moist and wet from 362 to 396 ft, and wet thereafter.

595 to 825 ft SILTY SAND with gravel (SM)**

SM layers up to 150 ft thick predominate. Several widely spaced, 5 ft thick well-graded sands with silt (SW-SM) are also present. The plasticity of fines in SM layers ranges from non-plastic to low plasticity. Gravel clasts are predominantly volcanic in origin and subrounded. Sediment color ranges from moderate yellowish brown (10YR 4/4) to dark yellowish brown (10YR 4/2) and no cementation or reaction to 10% HCl was observed. All samples were wet.

825 to 900 ft ASHFLOW TUFF

Homogeneous, dusky yellow colored (5Y 6/4), weakly welded, aphyric, unweathered tuff with an open/porous sugary texture. Trace amounts of colorless quartz crystals and trace amounts of pumice are present.

*Below approximately 420 ft percent fines measured in drill cuttings become markedly higher and percent gravel becomes markedly lower. It is probable that these changes are due to drilling impacts that were also observed in NC-EWDP-10SA and in -22SA. Therefore, some of the SM layers identified in this log interval based on drilling cutting samples may in fact be SW-SM under in situ conditions. This also is likely the case in the underlying depth interval from 595 to 825 ft.

**The presence of greater than 15 percent gravel throughout this interval is assumed based on the likelihood that drilling impacts that decrease gravel percentages in drill cuttings compared to in situ conditions in NC-EWDP-10SA and in -22SA are also operative in -19IM2A.

Nye County, Nevada Nuclear Waste Repository Project Office	
Early Warning Drilling Program Summary Lithology Log NC-EWDP-19IM2A	
Date: 12/20/02	Geologist: JSW
Scale: Not to scale	Drawn by: RFD

APPENDIX 2B-22SA Summary Lithology Log

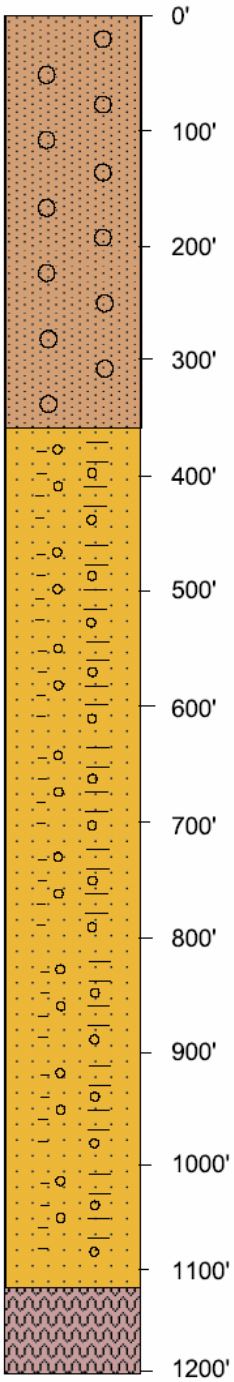

0 to 360 ft WELL-GRADED SAND with silt and gravel (SW-SM)

Thinly bedded SW-SM layers 5 to 25 ft predominate. Several thin lenses of well-graded gravel with silt and sand (GW-GM) less than 5 ft thick are also present in the interval. Gravel clasts are volcanic in origin and subangular to subrounded with rare rounded clasts. Sediment color is predominantly light to moderate brown (5YR 5/4). Moderate cementation is present from 0 to 22.5 ft and locally weak cementation is present 22.5 to 105 ft. Sediments displayed strong reaction to 10% HCl from 0 to 22.5 ft and locally weak to strong reaction to 105 ft. All samples were dry.

360 to 1110 ft SILTY SAND with gravel (SM)*

SM layers with gravel generally less than 80 ft thick predominate. Several layers of well-graded sand with silt and gravel (SW-SM) layers less than 10 ft thick are also present above 705 ft. Plasticity of fines in SM layers ranges from non-plastic to moderately plastic. Gravel clasts are volcanic in origin and subrounded to subangular. Sediment color ranges from moderate yellowish brown (10YR 5/4) to light brown (5YR 5/6) to moderate brown (5YR 5/4). Weak cementation is present from 690 to 750 ft, and moderate to strong cementation is present from 750 to 1110 ft. A weak reaction to 10% HCl was observed from 755 to 880 ft and a strong reaction from 880 to 1110 ft. Samples were dry to 452 ft, moist from 452 to 485 ft, and wet from 485 to 705 ft, moist from 705 to 790 ft, and wet from 790 to 1110 ft.

*USCS texture classification between 705 and 1110 ft is based on drill cuttings particle size distribution measurements from this borehole between 360 and 705 ft and on similar measurements on core samples from 7 core runs between 391 and 743 ft in NC-EWDP-22PA.

1110 to 1200 ft (T.D.) VOLCANIC CONGLOMERATE

Clasts range in color from moderate brown (5YR 4/4) to moderate yellowish brown (10YR 3/4) to dark yellowish brown (10YR 4/2). Clasts are well sorted, rounded to subrounded, and composed of welded ashflow tuff lithologies. The matrix is dark yellowish orange (10YR 6/6) clayey fine sand. HCl reaction is weak to moderately strong thoughout the interval.

Nye County, Nevada Nuclear Waste Repository Project Office	
Early Warning Drilling Program Summary Lithology Log NC-EWDP-22SA	
Date: 12/18/02	Geologist: JSW
Scale: Not to scale	Drawn by: RFD

APPENDIX 2C-10SA Summary Lithology Log

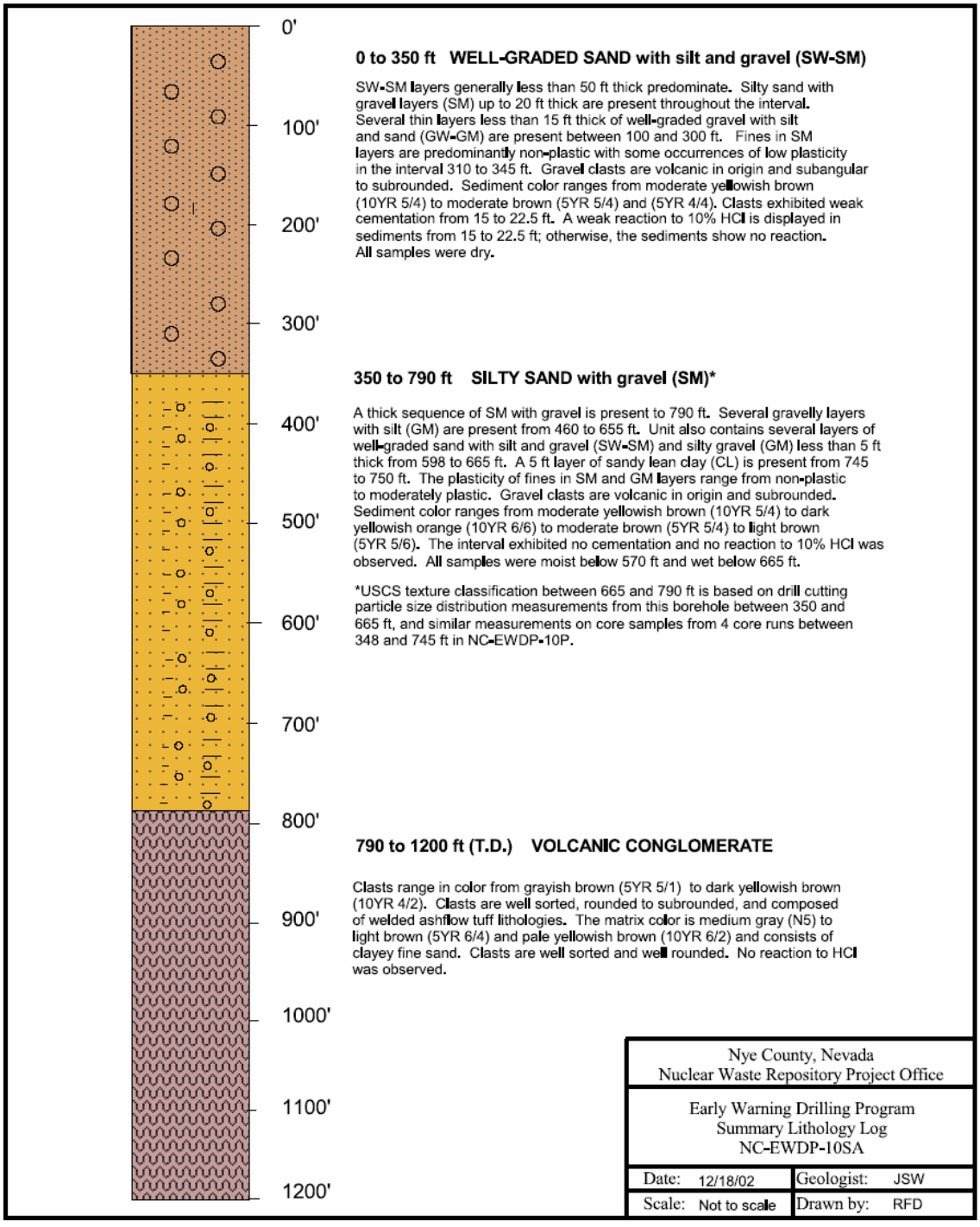

APPENDIX 3A-PHREEQC 19D Zone 1 Groundwater Geochemical Modeling Output

```
Input file: C:\DOCUME~1\182911\LOCALS~1\Temp\phreeqc.tmp
Output file: C:\Documents and Settings\182911\Desktop\Cindy Scism\UNM\PHREQC\19D Zone 1.out
Database file: C:\Program Files\Phreeqc\Phreeqc.dat

------------------
Reading data base.
------------------

      SOLUTION_MASTER_SPECIES
      SOLUTION_SPECIES
      PHASES
      EXCHANGE_MASTER_SPECIES
      EXCHANGE_SPECIES
      SURFACE_MASTER_SPECIES
      SURFACE_SPECIES
      RATES
      END
-----------------------------------
Reading input data for simulation 1.
-----------------------------------

      TITLE Speciation in 19D Zone 1 Groundwater
      SOLUTION 1  NC-EWDP-19D Zone 1 Groundwater
              units   ppm
              pH      8.6
              temp    25.0
              Ca              3.7
              Mg              0.31
              Na              91.5
              K               3.7
              Cl              6.7
              Alkalinity      189 as HCO3
```

```
              S(6)            22
              N(5)            2.21    as NO3

      END
-----
TITLE
-----

 Speciation in 19D Zone 1 Groundwater

-----------------------------------------
Beginning of initial solution calculations.
-----------------------------------------

Initial solution 1.     NC-EWDP-19D Zone 1 Groundwater

-----------------------------Solution composition------------------------------

      Elements           Molality       Moles

      Alkalinity        3.098e-03   3.098e-03
      Ca                9.234e-05   9.234e-05
      Cl                1.890e-04   1.890e-04
      K                 9.465e-05   9.465e-05
      Mg                1.275e-05   1.275e-05
      N(5)              3.565e-05   3.565e-05
      Na                3.981e-03   3.981e-03
      S(6)              2.291e-04   2.291e-04

----------------------------Description of solution----------------------------

                                     pH  =   8.600
                                     pe  =   4.000
                         Activity of water  =   1.000
                            Ionic strength  =   4.386e-03
                        Mass of water (kg)  =   1.000e+00
                    Total carbon (mol/kg)  =   3.033e-03
```

```
                    Total CO2 (mol/kg)  =   3.033e-03
                   Temperature (deg C)  =  25.000
                Electrical balance (eq)  =   5.049e-04
 Percent error, 100*(Cat-|An|)/(Cat+|An|)  =   6.31
                              Iterations  =   8
                                 Total H  = 1.110154e+02
                                 Total O  = 5.551633e+01

----------------------------Distribution of species----------------------------

                                                 Log       Log         Log
      Species            Molality    Activity  Molality  Activity     Gamma

      OH-               4.283e-06   3.985e-06    -5.368    -5.400    -0.031
      H+                2.680e-09   2.512e-09    -8.572    -8.600    -0.028
      H2O               5.551e+01   9.999e-01     1.744    -0.000     0.000
C(4)             3.033e-03
      HCO3-             2.932e-03   2.735e-03    -2.533    -2.563    -0.030
      CO3-2             6.743e-05   5.106e-05    -4.171    -4.292    -0.121
      CO2               1.543e-05   1.545e-05    -4.812    -4.811     0.000
      NaHCO3            5.681e-06   5.687e-06    -5.246    -5.245     0.000
      CaCO3             5.354e-06   5.359e-06    -5.271    -5.271     0.000
      NaCO3-            3.776e-06   3.516e-06    -5.423    -5.454    -0.031
      CaHCO3+           2.337e-06   2.180e-06    -5.631    -5.662    -0.030
      MgCO3             4.308e-07   4.312e-07    -6.366    -6.365     0.000
      MgHCO3+           3.041e-07   2.832e-07    -6.517    -6.548    -0.031
Ca               9.234e-05
      Ca+2              8.255e-05   6.248e-05    -4.083    -4.204    -0.121
      CaCO3             5.354e-06   5.359e-06    -5.271    -5.271     0.000
      CaHCO3+           2.337e-06   2.180e-06    -5.631    -5.662    -0.030
      CaSO4             2.099e-06   2.101e-06    -5.678    -5.677     0.000
      CaOH+             4.433e-09   4.128e-09    -8.353    -8.384    -0.031
      CaHSO4+           3.321e-14   3.092e-14   -13.479   -13.510    -0.031
Cl               1.890e-04

      Cl-               1.890e-04   1.759e-04    -3.723    -3.755    -0.031
```

H(0)		8.925e-29				
	H2	4.462e-29	4.467e-29	-28.350	-28.350	0.000
K		9.465e-05				
	K+	9.454e-05	8.797e-05	-4.024	-4.056	-0.031
	KSO4-	1.119e-07	1.042e-07	-6.951	-6.982	-0.031
	KOH	1.213e-10	1.214e-10	-9.916	-9.916	0.000
Mg		1.275e-05				
	Mg+2	1.166e-05	8.850e-06	-4.933	-5.053	-0.120
	MgCO3	4.308e-07	4.312e-07	-6.366	-6.365	0.000
	MgSO4	3.494e-07	3.497e-07	-6.457	-6.456	0.000
	MgHCO3+	3.041e-07	2.832e-07	-6.517	-6.548	-0.031
	MgOH+	1.374e-08	1.279e-08	-7.862	-7.893	-0.031
N(5)		3.565e-05				
	NO3-	3.565e-05	3.315e-05	-4.448	-4.480	-0.032
Na		3.981e-03				
	Na+	3.968e-03	3.698e-03	-2.401	-2.432	-0.031
	NaHCO3	5.681e-06	5.687e-06	-5.246	-5.245	0.000
	NaCO3-	3.776e-06	3.516e-06	-5.423	-5.454	-0.031
	NaSO4-	3.355e-06	3.124e-06	-5.474	-5.505	-0.031
	NaOH	9.715e-09	9.724e-09	-8.013	-8.012	0.000
O(0)		4.173e-36				
	O2	2.087e-36	2.089e-36	-35.681	-35.680	0.000
S(6)		2.291e-04				
	SO4-2	2.232e-04	1.686e-04	-3.651	-3.773	-0.122
	NaSO4-	3.355e-06	3.124e-06	-5.474	-5.505	-0.031
	CaSO4	2.099e-06	2.101e-06	-5.678	-5.677	0.000
	MgSO4	3.494e-07	3.497e-07	-6.457	-6.456	0.000
	KSO4-	1.119e-07	1.042e-07	-6.951	-6.982	-0.031
	HSO4-	4.421e-11	4.117e-11	-10.354	-10.385	-0.031
	CaHSO4+	3.321e-14	3.092e-14	-13.479	-13.510	-0.031

-------------------------------Saturation indices--------------------------------

Phase	SI	log IAP	log KT	
Anhydrite	-3.62	-7.98	-4.36	CaSO4

```
      Aragonite         -0.16   -8.50   -8.34  CaCO3
      Calcite           -0.02   -8.50   -8.48  CaCO3
      CO2(g)            -3.34   -4.81   -1.47  CO2
      Dolomite          -0.75  -17.84  -17.09  CaMg(CO3)2
      Gypsum            -3.40   -7.98   -4.58  CaSO4:2H2O
      H2(g)            -25.16   17.84   43.00  H2
      H2O(g)            -1.51   -0.00    1.51  H2O
      Halite            -7.77   -6.19    1.58  NaCl
      O2(g)            -32.79  -35.68   -2.89  O2

------------------
End of simulation.
------------------
```

APPENDIX 3B- PHREEQC 19D Zone 4 Groundwater Geochemical Modeling Output

```
Input file: C:\DOCUME~1\182911\LOCALS~1\Temp\phreeqc.tmp
Output file: C:\Documents and Settings\182911\Desktop\Cindy Scism\UNM\PHREQC\19D Zone 4.out
Database file: C:\Program Files\Phreeqc\Phreeqc.dat

------------------
Reading data base.
------------------

      SOLUTION_MASTER_SPECIES
      SOLUTION_SPECIES
      PHASES
      EXCHANGE_MASTER_SPECIES
      EXCHANGE_SPECIES
      SURFACE_MASTER_SPECIES
      SURFACE_SPECIES
      RATES
      END
-----------------------------------
Reading input data for simulation 1.
-----------------------------------

      TITLE Speciation in 19D Zone 4 Groundwater
      SOLUTION 1  NC-EWDP-19D Zone 4 Groundwater
              units   ppm
              pH      8.85
              temp    25.0
              Ca              0.92
              Mg              0.03
              Na              107.3
              K               3.4
              Cl              5.6
```

```
 Alkalinity      212 as HCO3
             S(6)            18.7
             N(5)            1.2    as NO3
      END
-----
TITLE
-----

 Speciation in 19D Zone 4 Groundwater

----------------------------------------
Beginning of initial solution calculations.
----------------------------------------

Initial solution 1.     NC-EWDP-19D Zone 4 Groundwater

-----------------------------Solution composition------------------------------

      Elements           Molality       Moles

      Alkalinity        3.476e-03   3.476e-03
      Ca                2.296e-05   2.296e-05
      Cl                1.580e-04   1.580e-04
      K                 8.698e-05   8.698e-05
      Mg                1.234e-06   1.234e-06
      N(5)              1.936e-05   1.936e-05
      Na                4.669e-03   4.669e-03
      S(6)              1.947e-04   1.947e-04

---------------------------Description of solution----------------------------

                                       pH  =   8.850
```

```
                                    pe  =   4.000
                       Activity of water  =   1.000
                          Ionic strength  =   4.740e-03
                       Mass of water (kg)  =   1.000e+00
                    Total carbon (mol/kg)  =   3.335e-03
                       Total CO2 (mol/kg)  =   3.335e-03
                     Temperature (deg C)  =  25.000
                  Electrical balance (eq)  =   7.619e-04
 Percent error, 100*(Cat-|An|)/(Cat+|An|)  =   8.66
                                Iterations  =   8
                                   Total H  = 1.110156e+02
                                   Total O  = 5.551706e+01

----------------------------Distribution of species----------------------------

                                                 Log       Log         Log
      Species            Molality    Activity  Molality  Activity     Gamma

      OH-               7.637e-06   7.086e-06    -5.117    -5.150    -0.032
      H+                1.511e-09   1.413e-09    -8.821    -8.850    -0.029
      H2O               5.551e+01   9.999e-01     1.744    -0.000     0.000
C(4)            3.335e-03
      HCO3-             3.176e-03   2.956e-03    -2.498    -2.529    -0.031
      CO3-2             1.309e-04   9.814e-05    -3.883    -4.008    -0.125
      CO2               9.378e-06   9.389e-06    -5.028    -5.027     0.000
      NaCO3-            8.503e-06   7.897e-06    -5.070    -5.103    -0.032
      NaHCO3            7.175e-06   7.183e-06    -5.144    -5.144     0.000
      CaCO3             2.412e-06   2.414e-06    -5.618    -5.617     0.000
      CaHCO3+           5.935e-07   5.523e-07    -6.227    -6.258    -0.031




MgCO3             7.714e-08   7.723e-08    -7.113    -7.112     0.000
      MgHCO3+           3.071e-08   2.852e-08    -7.513    -7.545    -0.032
```

Ca		2.296e-05				
	Ca+2	1.954e-05	1.464e-05	-4.709	-4.834	-0.125
	CaCO3	2.412e-06	2.414e-06	-5.618	-5.617	0.000
	CaHCO3+	5.935e-07	5.523e-07	-6.227	-6.258	-0.031
	CaSO4	4.166e-07	4.171e-07	-6.380	-6.380	0.000
	CaOH+	1.852e-09	1.720e-09	-8.732	-8.764	-0.032
	CaHSO4+	3.716e-15	3.451e-15	-14.430	-14.462	-0.032
Cl		1.580e-04				
	Cl-	1.580e-04	1.466e-04	-3.801	-3.834	-0.032
H(0)		2.822e-29				
	H2	1.411e-29	1.413e-29	-28.850	-28.850	0.000
K		8.698e-05				
	K+	8.690e-05	8.064e-05	-4.061	-4.093	-0.032
	KSO4-	8.708e-08	8.088e-08	-7.060	-7.092	-0.032
	KOH	1.977e-10	1.979e-10	-9.704	-9.703	0.000
Mg		1.234e-06				
	Mg+2	1.097e-06	8.247e-07	-5.960	-6.084	-0.124
	MgCO3	7.714e-08	7.723e-08	-7.113	-7.112	0.000
	MgHCO3+	3.071e-08	2.852e-08	-7.513	-7.545	-0.032
	MgSO4	2.756e-08	2.759e-08	-7.560	-7.559	0.000
	MgOH+	2.282e-09	2.119e-09	-8.642	-8.674	-0.032
N(5)		1.936e-05				
	NO3-	1.936e-05	1.795e-05	-4.713	-4.746	-0.033
Na		4.669e-03				
	Na+	4.650e-03	4.322e-03	-2.333	-2.364	-0.032
	NaCO3-	8.503e-06	7.897e-06	-5.070	-5.103	-0.032
	NaHCO3	7.175e-06	7.183e-06	-5.144	-5.144	0.000
	NaSO4-	3.329e-06	3.092e-06	-5.478	-5.510	-0.032
	NaOH	2.019e-08	2.021e-08	-7.695	-7.694	0.000
O(0)		4.173e-35				
	O2	2.086e-35	2.089e-35	-34.681	-34.680	0.000
S(6)		1.947e-04				
	SO4-2	1.909e-04	1.427e-04	-3.719	-3.845	-0.126
	NaSO4-	3.329e-06	3.092e-06	-5.478	-5.510	-0.032
	CaSO4	4.166e-07	4.171e-07	-6.380	-6.380	0.000

```
      KSO4-             8.708e-08   8.088e-08    -7.060    -7.092    -0.032
      MgSO4             2.756e-08   2.759e-08    -7.560    -7.559     0.000
      HSO4-             2.111e-11   1.960e-11   -10.676   -10.708    -0.032
      CaHSO4+           3.716e-15   3.451e-15   -14.430   -14.462    -0.032

------------------------------Saturation indices-------------------------------

      Phase               SI log IAP  log KT

      Anhydrite        -4.32   -8.68   -4.36  CaSO4
      Aragonite        -0.51   -8.84   -8.34  CaCO3
      Calcite          -0.36   -8.84   -8.48  CaCO3
      CO2(g)           -3.56   -5.03   -1.47  CO2
      Dolomite         -1.84  -18.93  -17.09  CaMg(CO3)2
      Gypsum           -4.10   -8.68   -4.58  CaSO4:2H2O
      H2(g)           -25.66   17.34   43.00  H2
      H2O(g)           -1.51   -0.00    1.51  H2O
      Halite           -7.78   -6.20    1.58  NaCl
      O2(g)           -31.79  -34.68   -2.89  O2

------------------
End of simulation.
```

APPENDIX 3C- PHREEQC 10SA Groundwater Geochemical Modeling Output

```
Input file: C:\DOCUME~1\182911\LOCALS~1\Temp\phreeqc.tmp
Output file: C:\Documents and Settings\182911\Desktop\Cindy Scism\UNM\PHREQC\10S.out
Database file: C:\Program Files\Phreeqc\Phreeqc.dat

------------------
Reading data base.
------------------

      SOLUTION_MASTER_SPECIES
      SOLUTION_SPECIES
      PHASES
      EXCHANGE_MASTER_SPECIES
      EXCHANGE_SPECIES
      SURFACE_MASTER_SPECIES
      SURFACE_SPECIES
      RATES
      END
-----------------------------------
Reading input data for simulation 1.
-----------------------------------

      TITLE Speciation in 10S Groundwater
      SOLUTION 1  NC-EWDP-10SA Groundwater
              units   ppm
              pH      7.78
              temp    25.0
              Ca              13
              Mg              2.5
              Na              43
              K               5.2
              Cl              6.9
```

```
Alkalinity      100 as HCO3
              S(6)            14
              N(5)            1.4    as NO3
      END
-----
TITLE
-----

 Speciation in 10S Groundwater

----------------------------------------
Beginning of initial solution calculations.
----------------------------------------

Initial solution 1.     NC-EWDP-10SA Groundwater

-----------------------------Solution composition------------------------------

      Elements           Molality       Moles

      Alkalinity        1.639e-03   1.639e-03
      Ca                3.244e-04   3.244e-04
      Cl                1.947e-04   1.947e-04
      K                 1.330e-04   1.330e-04
      Mg                1.028e-04   1.028e-04
      N(5)              2.258e-05   2.258e-05
      Na                1.871e-03   1.871e-03
      S(6)              1.458e-04   1.458e-04

---------------------------Description of solution----------------------------

                                       pH  =   7.780
```

```
                                    pe  =   4.000
                       Activity of water  =   1.000
                          Ionic strength  =   3.029e-03
                       Mass of water (kg)  =   1.000e+00
                  Total carbon (mol/kg)  =   1.688e-03
                     Total CO2 (mol/kg)  =   1.688e-03
                    Temperature (deg C)  =  25.000
                 Electrical balance (eq)  =   7.104e-04
 Percent error, 100*(Cat-|An|)/(Cat+|An|)  =  14.35
                                Iterations  =   8
                                   Total H  = 1.110141e+02
                                   Total O  = 5.551187e+01

----------------------------Distribution of species----------------------------

                                                 Log       Log         Log
      Species            Molality    Activity  Molality  Activity     Gamma

      OH-               6.409e-07   6.032e-07    -6.193    -6.220    -0.026
      H+                1.754e-08   1.660e-08    -7.756    -7.780    -0.024
      H2O               5.551e+01   9.999e-01     1.744    -0.000     0.000
C(4)             1.688e-03
      HCO3-             1.615e-03   1.523e-03    -2.792    -2.817    -0.026
      CO2               5.679e-05   5.682e-05    -4.246    -4.245     0.000
      CO3-2             5.444e-06   4.303e-06    -5.264    -5.366    -0.102
      CaHCO3+           5.083e-06   4.793e-06    -5.294    -5.319    -0.026
      CaCO3             1.782e-06   1.783e-06    -5.749    -5.749     0.000
      NaHCO3            1.506e-06   1.507e-06    -5.822    -5.822     0.000
      MgHCO3+           1.484e-06   1.397e-06    -5.829    -5.855    -0.026
      MgCO3             3.218e-07   3.220e-07    -6.492    -6.492     0.000
      NaCO3-            1.498e-07   1.410e-07    -6.825    -6.851    -0.026

Ca               3.244e-04
```

	Ca+2	3.122e-04	2.467e-04	-3.506	-3.608	-0.102
	CaSO4	5.329e-06	5.333e-06	-5.273	-5.273	0.000
	CaHCO3+	5.083e-06	4.793e-06	-5.294	-5.319	-0.026
	CaCO3	1.782e-06	1.783e-06	-5.749	-5.749	0.000
	CaOH+	2.619e-09	2.467e-09	-8.582	-8.608	-0.026
	CaHSO4+	5.506e-13	5.185e-13	-12.259	-12.285	-0.026
Cl		1.947e-04				
	Cl-	1.947e-04	1.832e-04	-3.711	-3.737	-0.026
H(0)		3.897e-27				
	H2	1.948e-27	1.950e-27	-26.710	-26.710	0.000
K		1.330e-04				
	K+	1.329e-04	1.251e-04	-3.876	-3.903	-0.026
	KSO4-	1.011e-07	9.523e-08	-6.995	-7.021	-0.026
	KOH	2.612e-11	2.613e-11	-10.583	-10.583	0.000
Mg		1.028e-04				
	Mg+2	9.903e-05	7.842e-05	-4.004	-4.106	-0.101
	MgSO4	1.990e-06	1.992e-06	-5.701	-5.701	0.000
	MgHCO3+	1.484e-06	1.397e-06	-5.829	-5.855	-0.026
	MgCO3	3.218e-07	3.220e-07	-6.492	-6.492	0.000
	MgOH+	1.822e-08	1.715e-08	-7.740	-7.766	-0.026
N(5)		2.258e-05				
	NO3-	2.258e-05	2.124e-05	-4.646	-4.673	-0.027
Na		1.871e-03				
	Na+	1.868e-03	1.760e-03	-2.729	-2.755	-0.026
	NaHCO3	1.506e-06	1.507e-06	-5.822	-5.822	0.000
	NaSO4-	1.015e-06	9.556e-07	-5.994	-6.020	-0.026
	NaCO3-	1.498e-07	1.410e-07	-6.825	-6.851	-0.026
	NaOH	7.001e-10	7.006e-10	-9.155	-9.155	0.000
O(0)		2.191e-39				
	O2	1.096e-39	1.096e-39	-38.960	-38.960	0.000
S(6)		1.458e-04				
SO4-2		1.373e-04	1.083e-04	-3.862	-3.965	-0.103

```
      CaSO4              5.329e-06   5.333e-06    -5.273    -5.273     0.000
      MgSO4              1.990e-06   1.992e-06    -5.701    -5.701     0.000
      NaSO4-             1.015e-06   9.556e-07    -5.994    -6.020    -0.026
      KSO4-              1.011e-07   9.523e-08    -6.995    -7.021    -0.026
      HSO4-              1.856e-10   1.748e-10    -9.731    -9.757    -0.026
      CaHSO4+            5.506e-13   5.185e-13   -12.259   -12.285    -0.026

------------------------------Saturation indices-------------------------------

      Phase               SI log IAP  log KT

      Anhydrite        -3.21   -7.57   -4.36  CaSO4
      Aragonite        -0.64   -8.97   -8.34  CaCO3
      Calcite          -0.49   -8.97   -8.48  CaCO3
      CO2(g)           -2.78   -4.25   -1.47  CO2
      Dolomite         -1.36  -18.45  -17.09  CaMg(CO3)2
      Gypsum           -2.99   -7.57   -4.58  CaSO4:2H2O
      H2(g)           -23.52   19.48   43.00  H2
      H2O(g)           -1.51   -0.00    1.51  H2O
      Halite           -8.07   -6.49    1.58  NaCl
      O2(g)           -36.07  -38.96   -2.89  O2

------------------
End of simulation.

------------------
```

APPENDIX 4-Summary of Experiments

Experiment 1A & 1B

Well I.D.: NC-EWDP-19IM1A

Interval (feet below ground surface): 740.0'-745.0'

Uranium Tracer Concentration: 1μM

Sorption Period: 09-17-2003-10/01/2003

Liquid/Solid ratio: 7.5

Desorption Period: 01/13/2004-05/26/2004

Desorption water: 19D Zone 1

Flow rates:

Time Interval (hrs)	Flow Rate (mL/hr)
0-80	8.00
81-175	4.00
176-342	3.00
343-387	2.80
388-441	1.00
442-708	0.50
709-3,206	0.40

Experiment 2A & 2B

Well I.D.: NC-EWDP-19IM1A

Interval (feet below ground surface): 740.0'-745.0'

Uranium Tracer Concentration: 1μM

Sorption Period: 12-23-2003-01/06/2004

Liquid/Solid ratio: 7.5

Desorption Period: 01/13/2004-04/25/2004

Desorption water: 19D Zone 4

Flow rates:

Time Interval (hrs)	Flow Rate (mL/hr)
0-53	4.00
54-720	1.00
721-2470	0.50

Experiment 3A & 3B

Well I.D.: NC-EWDP-10SA

Interval (feet below ground surface): 680.0'-685.0'

Uranium Tracer Concentration: 1μM

Sorption Period: 12-23-2003-01/06/2004

Liquid/Solid ratio: 7.5

Desorption Period: 07/07/2004-08/09/2004

Desorption water: 10SA

Flow rates:

Time Interval (hrs)	Flow Rate (mL/hr)
0-31	4.00
32-195	2.00
196-212	0.50

Experiment 4A & 4B

Well I.D.: NC-EWDP-22SA

Interval (feet below ground surface): 557.5'-560.0'

Uranium Tracer Concentration: 1μM

Sorption Period: 12-23-2003-01/06/2004

Liquid/Solid ratio: 7.5

Desorption Period: 07/07/2004-08/09/2004

Desorption water: 19D Zone 1

Flow rates:

Time Interval (hrs)	Flow Rate (mL/hr)
0-31	4.00
32-195	2.00
196-212	0.50

Experiment 5A & 5B

Well I.D.: NC-EWDP-22SA

Interval (feet below ground surface): 557.5'-560.0'

Uranium Tracer Concentration: 1μM

Sorption Period: 12-23-2003-01/06/2004

Liquid/Solid ratio: 7.5

Desorption Period: 01/13/2004-04/25/2004

Desorption water: 19D Zone 4

Flow rates:

Time Interval (hrs)	Flow Rate (mL/hr)
0-53	4.00
54-720	1.00
721-2470	0.50

APPENDIX 5-EPMA Procedure

Alluvium samples are separated into three particle size fractions, a fine fraction (<75 μm), a medium fraction (75 μm - 500 μm) and a coarse fraction (500 μm - 2000 μm). Polished alluvium thin sections are prepared (Figure 1) by mounting all three fractions on the same slide. The alluvium particles are affixed to the slide with an epoxy resin and polished to a thickness of approximately 23 μm. The thin sections are exposed to a 10^{-5} M depleted uranium solution by submerging the microscope slide in the solution inside a Teflon bottle. The bottle containing the depleted uranium solution and alluvium thin section slide was rotated on a shaker for a period of two weeks. The two-week time period is arbitrary depending on the time required for the sorbing species and the matrix to reach equilibrium. Sorption equilibrium is determined by a batch sorption kinetic experiment. The slides were then analyzed using a JEOL 8200 electron microprobe at the Department of Earth and Planetary Science/Institute of Meteoritics, University of New Mexico. The microprobe is equipped with 5 wavelength dispersive x-ray spectrometers (WDS) and an ultrathin-window energy dispersive spectrometer (EDS). Point analyses were conducted at 15 kV and 30 nA. Natural mineral standards from C.M. Taylor Corporation (Sunnyvale, CA) were used as calibration standards, except U, which was calibrated on a U-metal also from Taylor. Counting times on the samples were 20 seconds for major elements and 30 to 40 seconds for minor elements and 120 seconds for U. A ZAF correction program from Oxford was used to reduce the raw data. (Spilde, 2004) A copy of the Microanalysis Work Sheet is shown in Figure 2.

Figure 1-Digital picture of polished thin sections mounted on a microscope slide. The microscope slide dimensions are 45 mm x 25 mm x 1 mm. The alluvium thin sections imbedded in the slide with an epoxy resin are approximately 23 μm thick and 8 mm in diameter. The section on the far left is the coarse fraction, the middle section is the medium fraction and the far right section is the fine fraction.

Figure 2-Microanalysis Work Sheet. Details of the analytical conditions including information on measurement time for each element and voltage are shown below.

Microanalysis Work Sheet

Date: 11/1/09 Client: C. Seism - LANL Analyst: M. Spilde

Sample Description:

Analysis to be done:

Position/mount#	Probe Conditions	Files	Notes:
1)	KeV 15	Group: Clients	
2)	nA 30	Sample: Seism - LANL	
3)	Apt.	Conditions:	
4)	Fil. Sat:		
5)			
6)			

Mount: Metallurgical (3M150) Thin Section (6M150) Standard Holder

	Element Conditions									PHA					Std		
	Elem	Line	Channel	Xtal	Spec. Pos.	Hi Bk Pos (+)	Lo Bk Pos (-)	Meas. Time	Bkg. Time	Gain	Voltage	Base V.	Window V.	Diff/Int	Standard	~~Elem. Wt%~~	~~Calib. Date~~
1	Si	Kα	1	TAP		~~5~~ 9.5	6	20	10	16	1600	1.0	–	Int	Orthoclase		
2	Al	Kα	1	TAP		~~5~~ 4.5	5	20	10	16	1600	0.5	–	Int	Orthoclase		
3	Mg	Kα	3	TAPH		4	5	20	10	16	1600	0.5	4.5	Diff	Diopside		
4	Fe	Kα	4	LIFH		5	5	20	10	32	1750	1.0	6.0	Diff	Hematite		
5	Mn	Kα	4	LIFH		5	5	40	20	32	1750	0.7	6.0	Diff	Spessartine		
6	Ca	Kα	5	PET		5	6	20	10	8	1600	0.5	–	Int	Diopside		
7	Na	Kα	3	TAPH		5	5	30	15	16	1600	0.75	4	Diff	Albite		
8	K	Kα	5	PET		5	~~5~~ 7.0*	20	10	16	1580	0.5	–	Int	Orthoclase		
9	P	Kα	5	PET		5	5	30	15	16	1600	0.5	–	Int	Apatite		
10	U	Mα	2	PETL		3.5	4	100	50	32	1750	0.5	–	Int	U-metal		
11																	
12																	
13																	
14																	
15																	

Spectrometers					
	1	2	3 (H-type)	4 (H-type)	5
Crystals	LiF PET LAP LDE2	LPET	TAPH LDE3	LIFH PETH	LiF PET LAP LDE1
Detector	Gas Flow	Sealed	Gas Flow	Sealed	Gas Flow

Spectrometer Setup					
	1	2	3	4	5
Crystal					
Elements	Si Al	U	Mg Na	Fe Mn	Ca K P

* K Hi Bk overlaps w/ U Mα

Stds From C.M. Taylor Corp., Sunnyvale, CA

APPENDIX 6- EPMA Analytical Results

	Mass percent												
No.	SiO2	UO2	Na2O	MnO	P2O5	Al2O3	MgO	FeO	K2O	CaO	CO2	Total	Comment
3	64.922	0	0.982	0.007	0	16.396	0.006	1.739	15.917	0.006	0	99.975	Orthoclase std test 1
4	64.707	0	1.003	0.01	0.018	16.396	0	1.764	15.849	0	0	99.747	Orthoclase std test 2
5	0.395	19.543	0.002	0	0	0.043	0.035	0.044	0.117	0.076	318.207	338.462	1a coarse spot 1
6	0.422	13.431	0.003	0.125	0	0.072	0.024	5.433	0.081	0.038	0	19.629	1a coarse spot 2
7	0.814	14.501	0.008	0	0	0.09	0.051	0.086	0.096	0.05	0	15.696	1a coarse spot 3
8	0.153	12.021	0.01	0	0.005	0.028	0	0.033	0.055	0.024	0	12.329	1a coarse spot 4
9	63.695	0	6.363	0	0.001	23.128	0.032	0.558	2.648	3.658	0	100.083	1a coarse spot 5
10	12.876	0.012	0.013	0.003	0.023	7.706	0.812	70.696	0.145	0.194	0	92.48	1b coarse Fe-ox 1
11	4.336	0.009	0.013	0	0.005	2.117	0.291	89.237	0.095	0.122	0	96.225	1b coarse Fe-ox 2
12	4.367	0.028	0	0	0.009	3.076	0.14	87.193	0.077	0.133	0	95.023	1b coarse Fe-ox 3
13	10.268	0.027	0	0	0.016	8.996	0.081	76.473	0.065	0.091	0	96.017	1b coarse Fe-ox vein 4
14	6.326	0.017	0.002	0	0.023	5.395	0.064	85.343	0.05	0.08	0	97.3	1b coarse Fe-ox vein 5
15	4.094	0.032	0.02	0	0	3.155	0.069	88.325	0.046	0.071	0	95.812	1b coarse Fe-ox vein 6
16	46.274	0.14	0.627	0.025	0.243	15.388	1.955	2.157	1.996	1.102	0	69.907	1b coarse clay 7
17	26.081	0.031	0.005	0	0.004	5.262	0.505	41.76	0.189	0.149	0	73.986	1b coarse clay-Fe-Ox 8
18	91.805	0.004	0.013	0	0	2.571	0.006	0.151	0.154	0.052	0	94.756	1b coarse matrix 9
19	61.477	0	0.071	0	0.013	0.448	0.002	0.069	0.023	0.049	0	62.152	1b coarse matrix 10
20	9.915	0.007	0	0.003	0.013	6.71	0.36	77.18	0.063	0.23	0	94.481	1b coarse matrix 11
21	58.156	0.053	0.085	0.011	0.102	13.033	2.209	2.324	0.374	3.636	0	79.983	1 fine spot 1
22	39.067	0.441	0.523	0.027	0.076	3.287	0.466	1.162	0.661	1.118	0	46.828	1 fine spot 2
23	65.449	0.004	1.208	0.03	0.032	13.835	1.475	2.778	4.291	0.493	0	89.595	1 fine spot 3
24	52.446	0.016	0.652	0.229	0.248	15.172	2.141	3.709	1.436	1.932	0	77.981	1 fine spot 4
25	0.225	0.006	0.001	0.093	39.316	0	0.148	0.382	0.092	58.03	0	98.293	1b fine spot 1

26	70.256	0	2.187	0	0.027	11.535	0.191	1.283	3.597	0.769	0	89.845	1b fine spot 2
27	57.27	0	3.482	0.018	0.005	17.754	0	0.279	6.475	0.191	0	85.474	1b fine spot 3
28	67.437	0	5.287	0.01	0	13.475	0	0.218	1.251	0.795	0	88.473	1b fine spot 4
29	57.055	0.007	3.489	0.039	0.03	17.275	0.06	0.901	6.377	0.254	0	85.487	1b fine spot 5
30	57.844	0.009	5.9	0.012	0	17.918	0.033	0.595	4.475	0.53	0	87.316	1b fine spot 6
31	46.215	0.08	0.884	0.114	0.197	14.977	2.269	7.548	2.501	1.996	0	76.781	1b fine clay 7
32	0.364	0.04	0.009	1.244	0	0.007	0.011	153.035	0.029	0	0	154.739	2 medium Fe-ox 1
33	6.117	0.281	0.124	0.323	0.162	0.457	0.143	79.563	0.152	0.975	0	88.297	2 medium Fe-ox 2
34	4.043	0.033	0.058	0.228	0.115	0.403	0.189	86.99	0.116	0.614	0	92.789	2 medium Fe-ox 3
35	0.296	0.031	0	1.195	0	0	0	153.011	0.044	0.007	0	154.584	2 medium Fe-ox 4
36	3.863	1.703	0.115	0.556	0.359	0.215	0.027	73.027	0.188	1.032	0	81.085	2 medium Fe-ox 5
37	2.135	0.022	0.019	0.407	0.045	0.096	0.038	84.428	0.148	0.954	0	88.292	2 medium Fe-ox 6
38	4.378	0.373	0.083	0.551	0.063	0.309	0.197	84.815	0.262	0.396	0	91.427	2 medium Fe-ox 7
Minimum	0.153	0	0	0	0	0	0	0.033	0.023	0	0	12.329	
Maximum	91.805	19.543	6.363	1.244	39.316	23.128	2.269	153.035	15.917	58.03	318.207	338.462	
Average	29.598	1.747	0.923	0.146	1.143	7.131	0.39	37.897	1.948	2.218	8.839	91.981	
Sigma	29.253	4.812	1.748	0.304	6.544	7.227	0.691	47.21	3.868	9.61	53.035	50.969	
No. of data	36												

APPENDIX 7- EPMA Detection Limits

Element	Peak (mm)	Net (cps)	Bg-	Bg+	S.D.(%)	D.L. (ppm)	D.L. (wt %)
1 Si	77.715	1556.5	248.5	131.2	0.63	144	0.014
2 U	125.425	23.2	37.7	31.3	4.78	99	0.010
3 Na	128.504	15.2	64.1	54.3	13.88	77	0.008
4 Mn	146.277	52.6	72.7	53.3	4.02	113	0.011
5 P	197.327	7	8.1	6.3	12.05	120	0.012
6 Al	90.995	98.6	120.6	62.7	3.78	98	0.010
7 Mg	106.448	28	154.1	110	13.65	116	0.012
8 Fe	134.694	12240.5	88.8	74.6	0.2	184	0.018
9 K	120.024	29.6	40.6	16.7	7.32	98	0.010
10 Ca	107.8	174.1	51.1	37.1	2.09	129	0.013


Los Alamos
NATIONAL LABORATORY
EST.1943